Nickel(II) Complexes with Electron-Rich, Sterically-Hindered PNP Pincer Ligands Enable Uncommon Modes of Ligand Dearomatization

Sébastien Lapointe[†], Eugene Khaskin[†], Robert R. Fayzullin[‡], Julia R. Khusnutdinova*[†]

[†] Coordination Chemistry and Catalysis Unit, Okinawa Institute of Science and Technology Graduate University, 1919-1 Tancha, Onna-son, Okinawa, Japan 904-0495

[‡] Arbuzov Institute of Organic and Physical Chemistry, FCR Kazan Scientific Center, Russian Academy of Sciences, 8 Arbuzov Street, Kazan 420088, Russian Federation

ABSTRACT: We report the reactivity and characterization of hydride, methyl, and bromo Ni^{II} complexes with a new class of electron-rich and sterically hindered PNP pincer ligands, Me_4PNP^R (R = ^{i}Pr, ^{t}Bu), in which a classical metal-ligand cooperative mode of reactivity via CH_2 arm deprotonation is blocked by methylation. This enables new, uncommon modes of PNP ligand dearomatization that involve reactivity in the *para*-position of the pyridine ring. In particular, the reduction of $[(Me_4PNP^{iPr})Ni^{II}Me]B(Ar^F)_4$ with KC_8 leads to the formation of a new C–C bond via dimerization of two complexes through the *para*-position. This reactivity stands in sharp contrast to the previously reported bromo or chloro complexes, where stable Ni^I halogen moieties are formed. Computational analysis showed a greater propensity for ligand-centered radical formation for the presumed intermediate Ni^IMe species. Homolysis of the Ni^{II}-Me bond in $[(Me_4PNP^{iPr})Ni^{II}Me]B(Ar^F)_4$ leads to the formation of a Me radical detected by radical traps and Ni^I intermediates that can be trapped in the presence of halide ions to give previously characterized, stable Ni^I halogen complexes. In addition, treatment of bromo-complexes $[(Me_4PNP^R)Ni^{II}Br]BPh_4$ with a powerful hydride source, $LiBEt_3H$, leads to the reduction of the pyridine ring and the formation of Ni^{II} complexes with an anionic amide-donor reduced pincer ligand, although aromatic Ni^{II} hydride complexes could also be obtained with a weaker hydride source. We have observed that steric bulk at the phosphine donors controls the reactivity of the resulting $Ni^{II}H$ complexes. While *t*-Bu-substituted $[(Me_4PNP^{tBu})Ni^{II}H]Y$ (Y = BPh_4, $B(Ar^F)_4$) does not react with O_2, the less sterically hindered ^{i}Pr-substituted $[(Me_4PNP^{iPr})Ni^{II}H]Y$ reacts instantaneously to give an unstable superoxide adduct that can be observed by EPR.

INTRODUCTION

Pincer complexes have been a focus of organometallic research for multiple decades since their initial description and characterization by Shaw[1] and van Koten[2, 3] in the 1970s. Since then, pincer ligands have been modified in countless ways to improve the electronic and steric properties required for different applications, from catalytic reactions to small molecule activation and stabilization of high- and low-valent metal complexes. Some of the most well-known pincer motifs include the PCP,[4-15] POC(sp^2)OP,[16-22] POC(sp^3)OP,[23] POCN,[24-28] PNP,[29-37] PONOP,[38-45] PIMCOP,[46] and NNN[47-49] amongst others.

Catalytic applications of pincer complexes with precious and non-precious metals such as Pd, Pt, Ru, Co, and Ni have been studied extensively over the past several decades.[50-56] Among them, nickel pincer complexes have been widely used and studied, mostly because of their ease of preparation, the wide range of catalytic activity, and rich reactivity in small molecule activation.[57, 58] For example, nickel hydrides supported by pincer ligands are known to be active in hydroborations[59], hydrosilylations,[60, 61] dehydrogenative coupling of aldehydes,[62] reduction of CO_2,[22, 63] as well as reactivity with acetylene[64, 65] and other small molecules.[13, 66] In addition, alkyl complexes of nickel with pincer ligands are known to engage in insertion of CO_2[13, 67], reactivity with electrophiles[66], and carbon-halide bond activation.[68]

In pyridine-based PNP pincer complexes, one of the most common reactions/activation pathways involves deprotonation of the ligand's CH_2 arms. This leads to the formation of a dearomatized complex, which can sometimes engage in metal-ligand cooperative bond activation.[69] However, the drawback of the acidic phosphine arms' CH_2 groups is their high reactivity, which sometimes leads to irreversible ligand framework modification and/or prevents reactivity at the metal.[70]

Inducing metal-based reactivity may be instrumental in studying base metal-mediated small molecule activation. In particular, nickel complexes in the less common oxidation states of +1 and +3 have been implicated in CO_2 activation,[71, 72] O_2 reactivity,[57, 58] C–C coupling[73, 74] and methanogenesis in Ni-containing enzymes.[75, 76]

We have previously reported new, sterically hindered, electron-rich Me_4PNP pincer ligands,[77] in which four Me groups are introduced in the pincer "arms" to prevent dearomatization of the pyridine ring.[69, 70] We were able to obtain unusually stable Ni^I complexes, whose geometry is controlled by the steric properties of the ligand (i.e. ^{t}Bu vs. ^{i}Pr) (Scheme 1). EPR and DFT studies showed that these complexes have a metalloradical character with spin density essentially localized

Scheme 1. Formation of stable Ni^{I} complexes with different geometries as previously reported.[77]

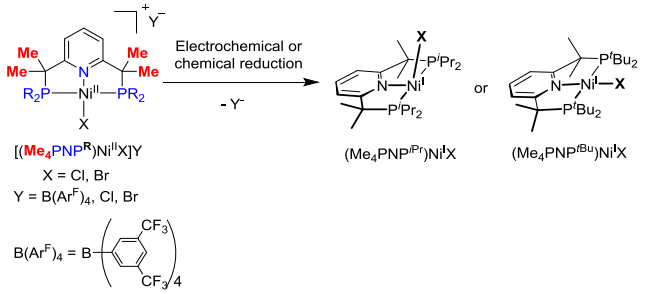

at the metal center, explaining the lack of reactivity at the ligand framework.

In this work, we set out to investigate nickel hydride and methyl complexes with Me_4PNP as these species possess a more electron-rich metal center and participate in classical reactions such as hydrogen activation. We wanted to study the effect of introducing steric bulk and the blocking of metal-ligand cooperativity on their reactivity in small molecule activation and in chemical reduction. We found that although traditional metal-ligand cooperativity at the pincer "arms" has been blocked, we were able to observe reactivity at the *para*-position of the pyridine ring in reactions with strong chemical reducing agents, leading to unusual types of pyridine ring dearomatization. We were also able to indirectly observe the formation of a transient, three coordinate Ni^{I} species through homolysis of the Ni–Me bond under strong UV irradiation. In traditional small molecule activation reactivity (CO, CO_2, ethylene, O_2), we found that introducing extreme steric bulk through ^{t}Bu substituents on the phosphine groups effectively blocks all reactivity, leading to exceptionally stable Ni hydride complexes that can be stored under air for several weeks, both in solution and the solid state, whereas the less bulky ^{i}Pr-substituted ligand does allow for O_2 reactivity, leading to the formation of a transient superoxide species.

RESULTS AND DISCUSSION

Synthesis and characterization of Ni^{II} complexes. The Ni^{II} complexes were prepared by reacting previously reported Ni^{II} halide complexes [(Me_4PNP^{R})NiBr]Br (R = ^{i}Pr, ^{t}Bu)[77] with either sodium tetraphenylborate ($NaBPh_4$) or sodium tetrakis[3,5-bis(trifluoromethyl)phenyl]borate ($NaB(Ar^{F})_4$) in dry THF to form [(Me_4PNP^{R})NiBr]BPh_4 (R = ^{i}Pr **[1]BPh_4**, ^{t}Bu **[2]BPh_4**) or previously reported [(Me_4PNP^{R})NiBr]$B(Ar^{F})_4$ (R = ^{i}Pr **[1]$B(Ar^{F})_4$**, ^{t}Bu **[2]$B(Ar^{F})_4$**)[77] (Scheme 2). Reacting these complexes with 10 equivalents of sodium borohydride ($NaBH_4$) in anhydrous THF over 4 to 18 hours produced hydride complexes [(Me_4PNP^{R})NiH]$B(Ar^{F})_4$ (R = ^{i}Pr **[3]$B(Ar^{F})_4$**, ^{t}Bu **[4]$B(Ar^{F})_4$**) and [(Me_4PNP^{R})NiH]BPh_4 (R = ^{i}Pr **[3]BPh_4**, ^{t}Bu **[4]BPh_4**) in high yields. Reacting complexes **[1]** and **[2]** with either methyllithium, lithium dimethylcuprate, or dimethylzinc over 5 minutes to 2 hours formed the methyl complexes [(Me_4PNP^{R})NiMe]$B(Ar^{F})_4$ (R = ^{i}Pr **[5]$B(Ar^{F})_4$**, ^{t}Bu **[6]$B(Ar^{F})_4$**) and [(Me_4PNP^{R})NiMe]BPh_4 (R = ^{i}Pr **[7]BPh_4**, ^{t}Bu **[8]BPh_4**) in 80% to 97% yield (See Scheme 2).

The use of $ZnMe_2$ resulted in clean and selective formation of the desired Ni-Me complexes after 2h, and the same complex could be obtained by a reaction with $CuMe_2Li$ after a shorter reaction time of only 5 min, albeit in a less selective manner. Although Ni–Me complex formation was also observed by using MeLi alone after ca. 1 h of reaction time, this reagent was the least selective among the three.

The ^{1}H NMR spectra for hydride complexes **[3]** and **[4]** show a hydride signal in the highly upfield region of -18 ppm as a triplet due to splitting from two phosphorous atoms ($J_{HP} \approx 55$ Hz). The methyl complexes **[5]** and **[6]** show the characteristic Me group signal from around 0 to -0.23 ppm split by two P atoms. The $^{13}C\{^{1}H\}$ spectra for the methyl complexes show the Ni-$\underline{C}H_3$ signal from -16 to -21 ppm. As observed previously for the halogen species, complexes that have bulky ^{t}Bu groups show broadened signals in ^{1}H NMR for the arm and phosphine methyls, caused by the hindered rotation of ^{t}Bu groups around the phosphine atom due to crowding from the methylated ligand arms.

Most complexes in this study have been analyzed by X-ray diffraction studies, NMR, HRMS and elemental analysis. Structural data for the complexes reported in Table 1 show almost ideal square planar geometry around the nickel center. The ORTEP diagrams of complexes **[3]BPh_4**, **[4]BPh_4**, **[5]BPh_4**, and **[6]BPh_4** are shown in Figure 1. All aromatized ^{i}Pr complexes show an "up-down" conformation in the crystals where one of the methyl groups on the arms is over the pyridine plane while the other is under the plane. This is also the case for all ^{t}Bu-substituted complexes except for complex **[2]BPh_4** (see below).

Scheme 2. Preparation of nickel(II) cationic complexes [1]-[6]

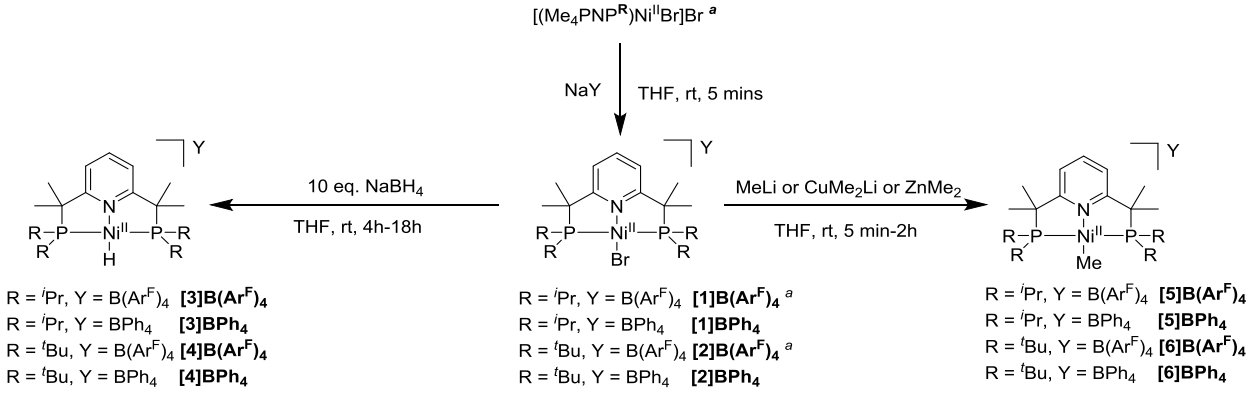

[a] Complexes were previously reported.[77]

Table 1. Bond distances [Å] and angles [deg] for complexes [1]-[6] according to XRD data.[a]

Complex	Ni1–N1	Ni1–X	Ni1–P1	Ni1–P2	∠ P1–Ni1–P2	∠ N1–Ni1–X	τ_4'[b]	τ_4[b]
[1]B(Ar^F)$_4$[c,d]	1.9095(13)	2.2827(2)	2.1786(4)	2.1805(4)	172.320(18)	176.66(4)	0.06	0.08
[1]BPh$_4$	1.9133(11)	2.2932(2)	2.1833(4)	2.1863(4)	173.064(15)	179.60(4)	0.03	0.05
[2]B(Ar^F)$_4$[c,e]	1.9236(15)	2.2877(12)	2.2324(12)	2.2454(13)	171.87(5)	178.84(7)	0.04	0.07
[2]BPh$_4$[e,f]	1.924(7)	2.2981(9)	2.2314(17)	2.2418(17)	171.40(7)	178.6(4)	0.05	0.07
[3]B(Ar^F)$_4$	1.9234(10)	1.45(2)	2.1424(3)	2.1366(3)	175.547(14)	179.3(8)	0.02	0.03
[3]BPh$_4$	1.9193(12)	1.367(19)	2.1297(4)	2.1468(4)	176.300(19)	178.7(8)	0.03	0.03
[4]B(Ar^F)$_4$[d]	1.9228(19)	1.34(3)	2.1430(6)	2.1452(6)	176.43(3)	179.9(18)	0.01	0.02
[4]BPh$_4$	1.9182(8)	1.469(15)	2.1555(2)	2.1574(2)	174.368(10)	178.4(6)	0.04	0.05
[5]B(Ar^F)$_4$	1.9567(9)	1.9471(11)	2.1691(3)	2.1619(3)	170.614(12)	178.03(5)	0.06	0.08
[5]BPh$_4$	1.9626(8)	1.9547(10)	2.1790(3)	2.1704(3)	170.919(10)	179.03(4)	0.04	0.07
[6]B(Ar^F)$_4$	1.9610(14)	1.9520(18)	2.2252(5)	2.2110(5)	171.544(19)	179.39(8)	0.04	0.06
[6]BPh$_4$	1.9515(13)	2.0012(15)	2.2085(4)	2.2072(5)	170.554(19)	178.30(7)	0.05	0.08

[a]Atom numbering corresponds to that of Figure 1; X = Br, H or Me. [b]Geometrical indexes τ_4' and τ_4 for the nickel centers are calculated according to refs.[78, 79] [c]Complexes were previously reported.[77] [d]There are two complexes in the asymmetric cell (Z' = 2); data are tabulated for the first one. [e] Data are listed for the main disordered component. [f]Data are tabulated for the experiment collected using Mo$K\alpha$ radiation.

As a result of multiple crystallization attempts, we were only able to obtain the structure of **[2]BPh$_4$** in the "up-up" conformation for both components of disorder, where two methyl groups are located over the pyridine plane, even though the very closely related complex with a B(Ar^F)$_4$ counterion crystalizes in the "up-down" conformation.[77] DFT analysis of the geometry-optimized structures show that "up-up" and "up-down" complexes are expected to have only a minor energy difference in vacuo, with the "up-up" isomer being only 2.11 kcal mol^{-1} higher in energy than the "up-down" isomer, well within the bound of error expected from DFT and also susceptible to small solid state energy differences due to crystal packing (see Supp. Info for details). Nevertheless, we cannot completely exclude the presence of an undetected disordered component with the "up-down" conformation in the crystals.

Reactivity of Ni^{II} complexes leading to pyridine ring dearomatization. Interestingly, while screening various hydride sources for the formation of Ni hydride complexes, we found that the reaction of bromide complexes **[1]BPh$_4$** and

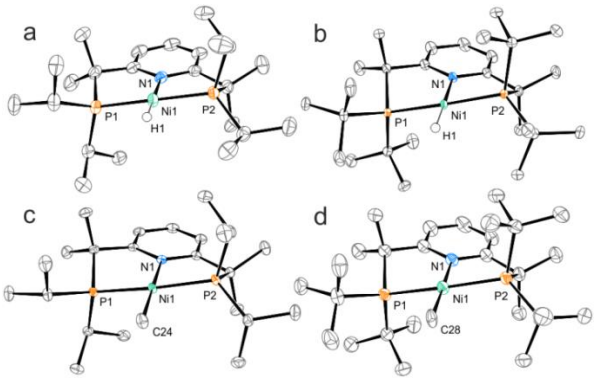

Figure 1. ORTEP diagrams of complexes **[3]BPh$_4$** (a), **[4]BPh$_4$** (b), **[5]BPh$_4$** (c), and **[6]BPh$_4$** (d) with the thermal ellipsoids set at 50% probability level. Most hydrogen atoms except for those on the nickel center, a minor disorder component for **[5]BPh$_4$**, and counterions are omitted for clarity.

Scheme 3. Synthesis of complexes 7-9

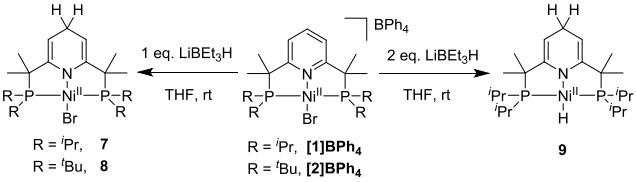

[2]BPh$_4$ with lithium triethylborohydride (LiBEt$_3$H, Superhydride) leads to ligand-based reactivity to give complexes **7** and **8** as major products, in which the pyridine ring is reduced, as evidenced from single crystal X-ray diffraction and NMR studies, while the Ni–Br bond remains intact (Scheme 3).

This reactivity resembles reduction of the pyridine ring in PONOP complexes with Superhydride reported by Jones et al.[42] and shows that in the presence of a strong reductant, the pyridine ring in our new, sterically-hindered PNP ligands displays non-innocent character.

Complex **7** was isolated in 87% yield while complex **8** was isolated in 77% yield, and they were both characterized by NMR, X-ray diffraction and HRMS. For complex **8**, 0.8 eq. of Superhydride was used instead of 1 equivalent because it furnished product of the higher purity, where unreacted starting material can be easily removed by filtration in diethyl ether.

When ^{i}Pr-substituted complex **[1]BPh$_4$** was treated with 2 equiv of LiBEt$_3$H, a new dearomatized hydride complex **9** was formed as a major product and characterized by NMR spectroscopy. Notably, when the ^{t}Bu-substituted analog **[2]BPh$_4$** was reacted with 2 equiv of LiBEt$_3$H under same conditions, a mixture of complex **8** as a major product and a presumed dearomatized hydride species as a minor product was observed by NMR spectroscopy (Figure S58). Lower reactivity of the ^{t}Bu-substituted analog compared to **[1]BPh$_4$** is likely due to a combination of steric and electronic factors preventing further nucleophilic substitution with LiBEt$_3$H.

Table 2. Bond distances [Å] and angles [deg] for complexes 7, 8, and 10 according to XRD data.[a]

Complex	Ni1–N1	Ni1–X	Ni1–P1	Ni1–P2	C1–C2	C2–C3	∠ P1–Ni1–P2	∠ N1–Ni1–X	τ_4'[b]	τ_4[b]
7[c]	1.8768(15)	2.3370(3)	2.1821(5)	2.1857(5)	1.337(3)	1.498(3)	170.67(2)	176.60(5)	0.07	0.09
8[d]	1.8810(12)	2.3071(3)	2.2297(4)	2.2205(4)	1.3386(19)	1.5060(19)	170.621(15)	178.29(4)	0.05	0.08
10[e]	1.9028(17)	1.954(2)	2.1510(6)	2.1585(6)	1.343(3)	1.509(3)	171.19(2)	177.29(9)	0.06	0.08

[a]Atom numbering corresponds to that of Figures 2 and 4; X = Br or Me. [b]Geometrical indexes τ_4' and τ_4 for the nickel centers are calculated according to refs.[78,79] [c]There are two complexes in the asymmetric cell (*Z'* = 2); data are tabulated for the first one. [d]Data are listed for the main disordered component; a hydride species is present as the minor disordered component with occupancy of 0.3331(10), and the Ni1–H1 bond length is 1.52(2) Å (see Supp. Info). [e]The asymmetric cell contains half of the molecule (*Z'* = 0.5); C3–C3^i 1.570(4) Å.

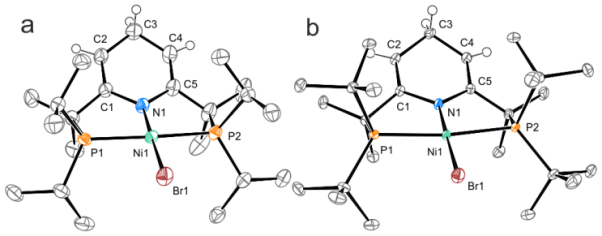

Figure 2. ORTEP diagrams of complexes **7** (a) and **8** (b) with the thermal ellipsoids set at 50% probability level. Hydrogen atoms except for those on the heterocycle are not shown. Complex **7** has two complexes in the asymmetric unit, only the first component is shown. Only the main component of the disorder is shown for complex **8**.

The X-ray diffraction study of complexes **7** and **8** revealed that the atom C3 deviates from the plane defined by atoms C1, C2, C4, C5, and N1 by 0.317(2) Å and 0.4470(15) Å, respectively, highlighting the loss of aromaticity of the heterocyclic moiety. The Ni1–N1 bond lengths for complexes **7** and **8** of 1.8768(15) Å and 1.8810(12) Å are shorter than their parent complexes **[1]BPh$_4$** and **[2]BPh$_4$**, with Ni1-N1 bond lengths of 1.9133(11) Å and 1.924(7) Å, respectively. The dearomatization of the pyridine ring can be seen by the shorter bond length for C1–C2 and C4–C5 compared to C2–C3 and C3–C4. For complex **7**, C1–C2 and C4–C5 bond lengths have double bond character with 1.337(3) and 1.338(3) Å bond distances, while C2–C3 and C3–C4 have single bond character with 1.498(3) and 1.497(3) Å bond distances. Similar bond lengths are present in complex **8**, with C1–C2, C4–C5 displaying double-bond character with 1.3386(19) and 1.3437(19) Å, while C2–C3, C3–C4 have structural single-bond character with 1.5060(19) and 1.5055(19) Å. The dearomatization of the pyridine ring is also evident from solution NMR of **7** and **8**, which shows upfield shifts for the heterocycle protons that now appear in the range of 2.8 to 4.2 ppm.

The propensity of our sterically bulky ligands to reduction at the *para* position is a feature that was originally not entirely desirable as the ligands were usually designed to prevent metal-ligand cooperation/dearomatization pathways, but also not entirely unexpected due to Jones' earlier PONOP report.[42] However, as mentioned previously, it was possible to obtain all the non-dearomatized hydride species with a less reducing $NaBH_4$ reagent cleanly. It is worth to consider that Superhydride reduction of the pyridine ring in the *para* position eventually provides a pathway for *in situ* formation of an anionic PNP ligand, which, as suggested by previous literature, might eventually enable different reactivity pathways as compared to neutral PNP ligands.[71, 80] Such pyridine reduction reactivity also resembles the NAD^+/NADH redox couple in biological systems and NADH-model compounds that are used as a reservoir of hydride ions.[81-83] The *para* position reactivity of the hydrides suggested that we may be able to get different outcomes upon electrochemical or chemical reduction of complexes **5-6** as compared to the halogen complexes and their associated stable and unreactive Ni^IX (X= Br, Cl) species earlier reported by us.[77]

Reactivity of Ni^{II}(Me) complexes with strong reductants leading to pyridine ring dearomatization. Accordingly, we next studied the reactivity of Ni^{II} methyl complexes with strong chemical reductants. Previously, we reported that Ni^{II} bromide and chloride complexes could be reduced by cobaltocene to form stable paramagnetic Ni^I complexes. In the case of Ni^{II}–Me complexes, cobaltocene was not a sufficiently strong reductant and no reduced product could be observed. Cyclic voltammetry studies gave us more insight into the different reactivity of these complexes when compared to their halide counterparts (Figure 3, a). For example, the reduction potential of complex **[5]B(Ar^F)$_4$** (−1.72 V) is much more negative than the reduction potential of cobaltocene, at around −1.33 V (in CH_2Cl_2)[84]. The reduction wave of complex **[5]B(Ar^F)$_4$** is electrochemically irreversible (ΔE_p = 0.54 V), suggesting that a Ni^I–Me species might be unstable after generation, or that it undergoes significant changes upon oxidation.[85]

The cyclic voltammogram of **[6]BPh$_4$** showed a quasireversible reduction wave at a less negative potential (−1.21 V) indicating that the presence of bulky ^{t}Bu-substituents might contribute to greater stabilization of the initial reduced product, at least on the electrochemical timescale.

For comparison, cyclic voltammograms of hydride complexes **[3]B(Ar^F)$_4$** and **[4]BPh$_4$** show completely irreversible reduction waves at very negative potentials, −2.39 and −2.42 V respectively, suggesting that the reduction products are likely unstable and very strong reductants are required for chemical reduction[84, 85] (Figure 3, b and Table 3).

Attempted reduction of **[3]B(Ar^F)$_4$** and **[4]BPh$_4$** by using 1 equivalent of a strong reductant, KC_8, initially gives a mixture paramagnetic products, as observed by EPR spectroscopy (See Figures S118 and S119). According to NMR analysis of the reaction mixtures, a complex mixture of diamagnetic products is eventually formed during the reduction of **[3]B(Ar^F)$_4$** and **[4]BPh$_4$**; free ligand was also present among the reaction products after reduction of **[3]B(Ar^F)$_4$**. We were unable to identify the products of reduction of hydride complexes due to their low stability.

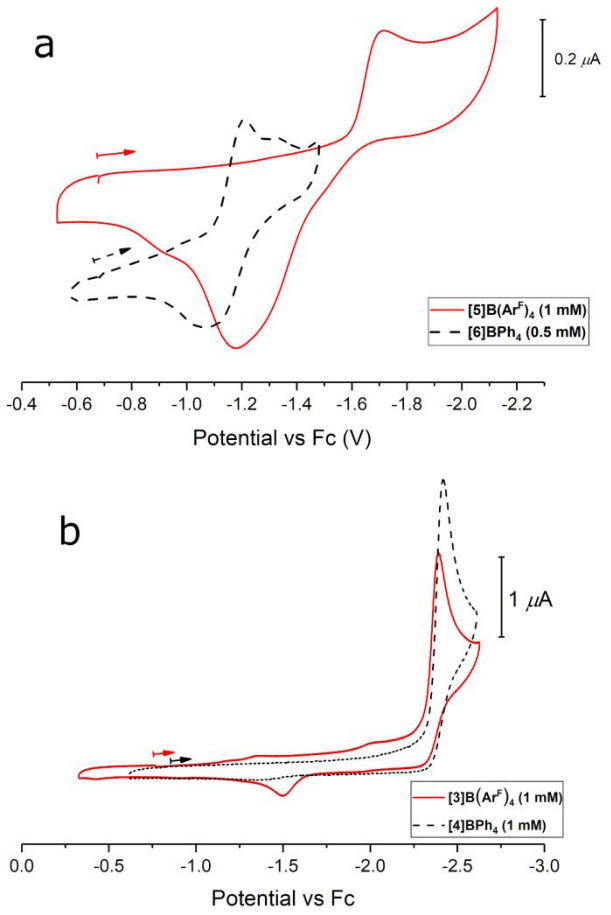

Figure 3. Cyclic voltammograms of Ni methyl and hydride complexes in the cathodic region: a) complexes **[5]B(Ar^F)$_4$ (**1 mM; red line**)** and **[6]BPh$_4$** (0.5 mM, dashed black line); b) complexes **[3]B(Ar^F)$_4$** (1 mM; red line) and **[4]BPh$_4$** (1 mM; dashed black line). Experimental conditions: 0.1 M ^{n}Bu$_4$NPF$_6$/MeCN solution at 23 °C, scan rate 0.1 V s^{-1}, 1.0 mm GC disk working electrode; the arrow indicates initial scan direction.

Table 3. Electrochemical properties of complexes [3]B(Ar^F)$_4$, [4]BPh$_4$, [5]B(Ar^F)$_4$ and [6]BPh$_4$.[a]

Complex	E_{pf} (V)[b]	E_{pr} (V)[c]	ΔE (V)[d]	$E_{1/2}$ (V)[e]
[3]B(Ar^F)$_4$	-2.389	-	-	-
[4]BPh$_4$	-2.422	-	-	-
[5]B(Ar^F)$_4$	-1.720	-1.180	0.540	-
[6]BPh$_4$	-1.209	-1.075	0.134	-1.142

[a]Cyclic voltammograms for complexes **[3]B(Ar^F)$_4$** (1 mM), **[4]BPh$_4$** (1 mM), **[5]B(Ar^F)$_4$** (1 mM) and **[6]BPh$_4$** (0.5 mM) in a 0.1 M solution of ^{n}Bu$_4$NPF$_6$ as supporting electrolyte in MeCN at 23°C; 100 mV/s scan rate; GC disk electrode (d = 1.6 mm); all peaks were referenced versus ferrocene. [b]Potential of the forward peak. [c]Potential of the return peak. [d]The peak-to-peak separation ΔE was calculated as E_{pf} - E_{pr}. [e]$E_{1/2}$ was estimated as ½(E_{pf} + E_{pr})

Interestingly, chemical reduction of the Ni^{II}–Me complex **[5]B(Ar^F)$_4$** with a very strong reductant (KC$_8$, potassium graphite) led to the formation of a new diamagnetic complex **10**, which was isolated in 33% yield and characterized by X-ray crystallography and NMR spectroscopy. According to the X-ray structure shown in Figure 4, **10** is a dimer, with a new C–C bond formed in the *para*-position of the pyridine rings, leading to overall pyridine ring reduction and dearomatization.

Similar to the dearomatized complex **7**, complex **10** shows bent heterocycle rings, and double bond character between the *ortho* and *meta* carbons. The geometry around the nickel center is also close to an ideal square planar geometry. The atom C3 deviates from the plane defined by atoms C1, C2, C4, C5, and N1 by a distance of 0.4235(19) Å. The C3–C3^i bond length of 1.570(4) Å is longer than the C2–C3 (1.509(3) Å) and C3–C4 (1.505(3) Å) single bonds in the pyridine ring, which are longer than the olefinic C1–C2 (1.343(3) Å) and C4–C5 (1.341(3) Å) bonds. NMR analysis of complex **10** shows that the heterocyclic protons are also significantly upfield shifted from the parent complex and fall in the range of 4.5 to 3.6 ppm, consistent with pyridine ring dearomatization.

This result shows that the reactivity of complex **[5]B(Ar^F)$_4$**, with its more electron-rich Ni–Me center, is predominantly ligand-based. In the previously reported Ni^{II} bromide and chloride complexes metal-based reduction was observed exclusively. The reasons behind ligand-based reactivity observed for Ni–Me complexes were analyzed through computational studies and are discussed below in more detail.

The attempted reduction **[6]BPh$_4$** with KC$_8$ under the same conditions afforded a mixture of paramagnetic products, however, these products could not be characterized or isolated in a pure form. Increased steric bulk in **[6]BPh$_4$** could prevent dimerization and clean formation of the C-C coupled dimer analogous to **10**, thus leading to other degradation pathways of the initial reduced product (see computational analysis below).

Scheme 4. Reduction of Nickel(II) methyl complex [5]B(Ar^F)$_4$ to form 10.

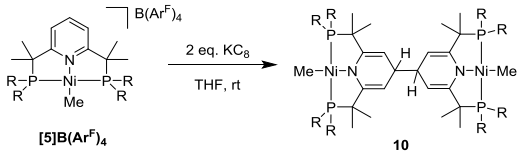

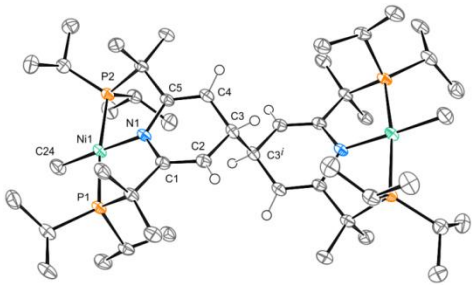

Figure 4. ORTEP diagram of complex **10** with the thermal ellipsoids set at 50% probability level. Hydrogen atoms except for those on the heterocycle are not shown. Selected interatomic distances (Å) and angles (deg.): Ni1–N1 1.9028(17), Ni1–C24 1.954(2), Ni1–P1 2.1510(6), Ni1–P2 2.1585(6), N1–C1 1.405(3), N1–C5 1.408(3), C1–C2 1.343(3), C2–C3 1.509(3), C3–C4 1.505(3), C4–C5 1.341(3), C3–C3^i 1.570(4), ∠P1–Ni1–P2 171.19(2), ∠N1–Ni1–C24 177.29(9). Equivalent atoms are labeled with the superscript *i* (–*x*, 1–*y*, 1–*z*).

UV-induced homolysis of Ni^{II}-Me bond. An alternative way to access a transient Ni^I species from an organometallic Ni^{II} complexes would be a homolysis of a Ni–C bond.[86] We inves-

tigated the reactivity of Ni^{II}-Me complexes **[5]B(Ar^F)$_4$** and **[6]B(Ar^F)$_4$** under irradiation by mercury lamp at RT in an acetone solution in the presence or absence of radical traps. Interestingly, initial trial experiments where we irradiated the solution of **[5]B(Ar^F)$_4$** without any additives produces a pink-colored solution already after 5 min.

To confirm whether Ni^{II}–Me bond homolysis occurs under these conditions, we performed the experiment in the presence of 5,5-dimethyl-1-pyrroline N-oxide (DMPO) as a radical trap, which could help to detect a transient Me radical. When we performed the irradiation for 1 hour at room temperature in the presence of an excess of DMPO, we observed a new signal of a DMPO-methyl adduct with g = 2.007, A_N = 14.25 G and A_H = 21.10 G (Figure 5, Scheme 5). The superhyperfine splitting parameters of the trapped radical are similar to those reported in the literature for a DMPO-Me radical adduct in acetone (A_N = 14.2 G, A_H = 21.6 G in acetone under gamma irradiation).[87]

When the solution of **[5]B(Ar^F)$_4$** was irradiated in the absence of a radical trap, the low temperature EPR spectrum showed only a weak signal with g values in the range from 2.17 to 2.04 (See Figure S114), which might indicate possible formation of metalloradical Ni^I species. However, the low intensity of the signal suggests that in the absence of stabilizing ligands, the resulting cationic Ni^I is likely to be unstable and to undergo further transformations. This transient Ni species could be either a T-shaped three-coordinate Ni^I species similar to those reported by the Lee[88] or Gade[57] groups or a solvent-stabilized tetracoordinate species.

In order to reliably detect the formation of possible Ni^I species, we performed the reaction in the presence of Br^- or Cl^- ions that can act as stabilizing ligands to form previously characterized stable (Me_4PNP^{iPr})Ni^IBr or (Me_4PNP^{iPr})Ni^ICl complexes, respectively (Scheme 5). To our satisfaction, irradiation of an acetone solution of **[5]B(Ar^F)$_4$** in the presence of 1 equiv. of ^{n}Bu$_4$NBr for 1h gave a pink-colored solution, whose EPR spectrum at 95 K shows a new rhombic signal with g-values of 2.328, 2.307, and 1.998, close to the g-values of the previously characterized (Me_4PNP^{iPr})Ni^IBr complex (g = 2.316, 2.309, and 1.993).[77] Similarly, a rhombic signal (g = 2.329, 2.307, and 1.998) was also observed in the presence of 1 equiv. of ^{n}Bu$_4$NCl, although the reaction was less clean (See Supporting Information).

Scheme 5. UV-induced reactivity of [5]B(Ar^F)$_4$.

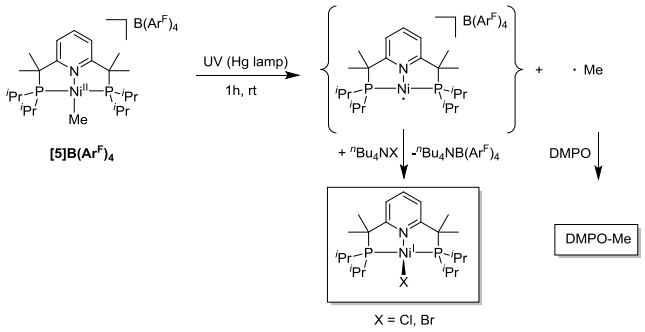

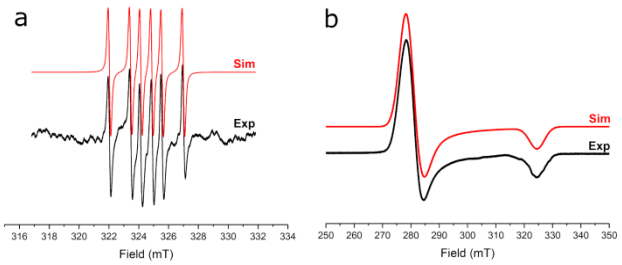

Figure 5. Experimental (black line) and simulated (red line) EPR spectra after UV irradiation of a) **[5]B(Ar^F)$_4$** after UV irradiation for 1 h at 298 K in the presence of excess DMPO; b) **[5]B(Ar^F)$_4$** in the presence 1 equiv of ^{n}Bu$_4$NBr after UV irradiation for 1h at 95 K. Parameters for simulation: a) g = 2.007, A_N = 14.25 G, A_H = 21.10 G. b) g_x = 2.328, g_y = 2.307, g_z = 1.998 (g_{iso} = 2.211).

In direct contrast with the less bulky ^{i}Pr substituents, when ^{t}Bu substituted complex **[6]B(Ar^F)$_4$** was irradiated in the presence of DMPO trap, we could not observe clean Ni–Me homolysis reactivity. No signals of DMPO-Me adduct were evident, with only a low intensity broad isotropic signal with a g-value of 2.164 observed (See Figure S115 in SI).

NMR analysis of **[6]B(Ar^F)$_4$** under UV irradiation shows eventual decomposition on the ligand framework as is seen by multiple new weak signals in the aromatic and aliphatic regions. However, the signal of the methyl group at around 0.13 ppm remains, showing that the Ni–Me bond persists.

Small molecule activation reactivity. We hypothesized that introducing significant steric hindrance through the influence of four Me groups and ^{t}Bu or ^{i}Pr substituents at the phosphines might alter the reactivity of the nickel methyl and hydride complexes towards small molecule activation. Indeed, the attempted reactions of complexes **[3]X**, **[4]X**, **[5]X**, and **[6]X** (X = B(Ar^F)$_4$ or BPh_4) with CO, CO_2, and ethylene failed to give significant amounts of any adducts or insertion products even up to 24 hours at 50 °C. Some minor degradation was observed upon prolonged heating of **[3]BPh$_4$** under CO atmosphere for 8 h, however, no CO adducts could be detected by IR spectroscopy. The nature of the counter anion, B(Ar^F)$_4$ or BPh_4, did not affect the reactivity.

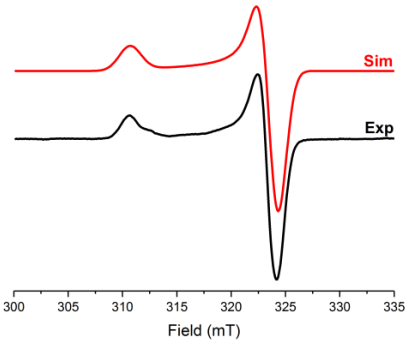

Figure 6. Experimental (black line) and simulated (red line) EPR spectra of the complex formed from the reaction of **[3]B(ArF)$_4$** with O_2 in frozen acetone at 84K. Parameters for simulation: $g_\perp$ = 2.003, $g_\parallel$ = 2.088

Reactivity of complexes 3-6 with oxygen. We then set out to study the reactivity of Ni hydride complexes with O_2, to determine if any oxygen adducts can be detected. The less sterically hindered ^{i}Pr-substituted complex **[3]BPh$_4$** readily reacts

with O_2 in a deuterated acetonitrile solution, which leads to an immediate solution color change from light yellow to red then quickly to orange within a few minutes. The first species observed by ^{1}H NMR 2 minutes after reaction with O_2 appears to be partially paramagnetic; the disappearance of a characteristic Ni–H signal can also be observed. Upon prolonged reaction time, the paramagnetic species disappears to reveal only a mixture of unidentified diamagnetic complexes. (Figures S70-S71 in SI)

The EPR spectrum recorded after reacting **[3]B(Ar^F)$_4$** with O_2 for 1 hour shows an axial signal with $g_\parallel$ and $g_\perp$ values of 2.088 and 2.003, respectively (Figure 6). These g-values that remain close to 2 are similar to the signals reported for known Ni superoxide complexes with NNN pincer ligands described by Gade et al.[58] We also recorded the EPR spectrum of the reaction of **[3]B(Ar^F)$_4$** with O_2 in the presence of an excess of DMPO, and obtained the spectrum shown in Figure S113 of supporting information with superhyperfine splitting constants (A_N = 13.2 G, A_H = 8.11 G, g = 2.0025), resembling those reported for characterized or proposed metal-superoxide adducts (for example, Co superoxide DMPO adduct, A_N = 12.8 G, A_H = 7.68 G, g = 2.008).[89] Although we could not isolate or further characterize the product of the reaction with O_2 due to its low stability and further decomposition, we propose that the formation of a similar Ni superoxide complex could occur in this case.[89, 90]

Interestingly, although Ni^{II} hydrides are usually considered to be highly reactive species, highly sterically hindered ^{t}Bu-substituted Ni^{II} hydride **[4]BPh$_4$** was stable under air or pure O_2 atmosphere for at least 24 hours according to ^{1}H and ^{31}P{^{1}H} NMR studies (Figures S72-S73 in SI). The Ni^{II} methyl complexes **[5]B(Ar^F)$_4$** and **[6]B(Ar^F)$_4$** did not react with O_2 even after 24 hours at 50° C.

These results demonstrate that controlling steric bulk of the pincer ligands leads to drastic differences in the stability and the reactivity towards small molecule activation. Imposing significant steric hindrance can lead to stabilization of normally highly reactive Ni–H and Ni–Me species in the presence of an O_2 atmosphere.

Computational studies of the reactivity of (Me$_4$PNP^R)Ni complexes. To shed light on the difference in reactivity of Ni^{II} halide, which leads to stable Ni^I complexes, and the reactivity of Ni^{II} methyl complexes that leads to dimerization through the *para*-position of the pyridine ring, we performed frontier orbital analysis of the cationic species **[5]$^+$** and **[6]$^+$** as well as tentative one-electron reduced neutral radical species **[5]$^\bullet$** and **[6]$^\bullet$** (Figure 7) and analyzed their spin density distribution (Figure 8).

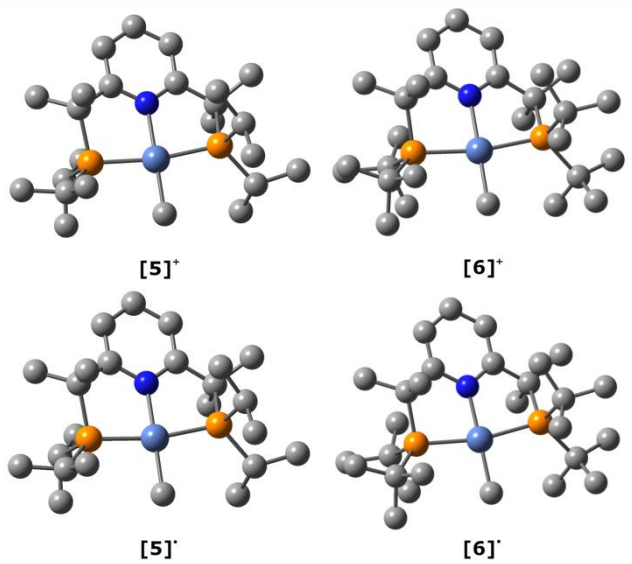

Figure 7. DFT-optimized structures of cationic Ni^{II}-Me **[5]$^+$** (a), **[6]$^+$** (c) and their one-electron-reduced products, neutral species **[5]$^\bullet$** (b), **[6]$^\bullet$** (d) (DFT optimized geometry. B3LYP, 6-311++G**/lanl2dz(Ni)).

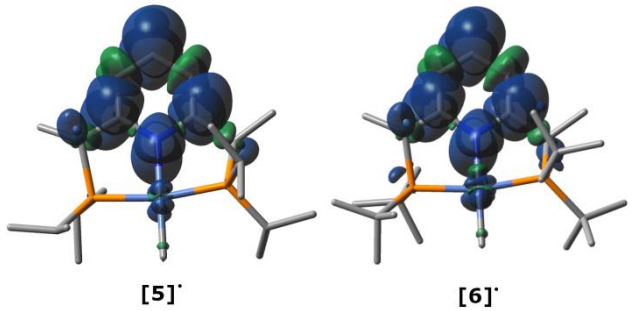

Figure 8. Spin density plots for complexes **[5]$^\bullet$** (a) and **[6]$^\bullet$** (b) (DFT optimized geometry, B3LYP, 6-311++G**/lanl2dz(Ni), isovalue = 0.0007).

Frontier orbital analysis shows that the LUMO of starting unreduced complexes **[5]$^+$** and **[6]$^+$** (Figure 9) essentially has a pyridine-based character, while the HOMO is metal based, with a mostly d_{z^2} character. By contrast, in complexes **[5]$^\bullet$** and **[6]$^\bullet$** the spin density is predominantly localized at the ligand, with highest spin density at the *para*-carbon positions of the pyridine rings (0.492 and 0.47, respectively), while the spin density at the Ni centers was found to be close to zero.

Previously, we reported that the spin density in neutral (Me$_4$PNP^R)NiX complexes (R = ^{i}Pr or ^{t}Bu; X = Br or Cl; analogues of **[5]$^\bullet$** and **[6]$^\bullet$**) is largely localized at the metal center, which is consistent with EPR studies that showed metal-based radical character.[77]

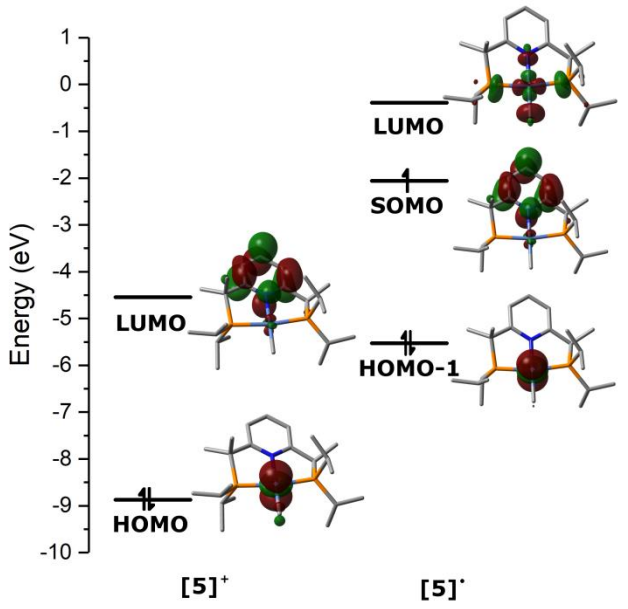

Figure 9. Molecular orbital diagram and HOMO, SOMO, and LUMO representation of **[5]**$^{+}$ and **[5]**$^{\bullet}$ (DFT optimized geometries, B3LYP, 6-311++G**/lanl2dz(Ni), alpha orbital representations, isovalue = 0.04).

Therefore, if one-electron reduction of **[5]**$^{+}$ and **[6]**$^{+}$ leads to the initial formation of transient **[5]**$^{\bullet}$ and **[6]**$^{\bullet}$, it is expected that the resulting ligand-based radical character will lead to their dimerization, which was observed experimentally for **5**. The localization of the spin density at the ligand as opposed to the metal is likely due to the more electron-rich alkyl ligand vs. halogens.

In addition, to explain the lack of reactivity of the Ni–methyl complexes towards CO, CO_2, and ethylene, we tried to optimize the geometry of the tentative five-coordinate adduct of (Me_4PNP^R)Ni^{II}Me with CO as a model compound, using various initial geometries (square pyramid or trigonal bipyramid) and different orientations of CO relative to the complex coordination planes (See Figures S145-S146). In the case of the square pyramid starting geometry with the CO in the "up" fashion **([5]CO-up** and **[6]CO-up**), no stable adducts with CO could be found, and CO remained outside of coordination sphere of the metal after optimization (Ni–C distance exceeding 5 Å), which is an uphill process with ΔG of 5.8 kcal·mol^{-1} for ^{i}Pr and 6.3 kcal·mol^{-1} for ^{t}Bu . In case of the same geometry with the CO in the "down" fashion (**[5]CO-down** and **[6]CO-down**) as well as the starting geometry where the CO is in in a trigonal bipyramidal fashion (**[5]CO-bipy** or **[6]CO-bipy**), the geometry of tentative CO adducts showing Ni–C distances of 2.18-2.24 Å were optimized. However, in all cases binding of CO was found to be an uphill process with ΔG of 14.7 kcal·mol^{-1} or 18.6 kcal·mol^{-1}, with the highest energy belonging to a ^{t}Bu complex (see Figures S147-S148).

SUMMARY AND CONCLUSION

We showed that designing the PNP pincer ligand in which dearomatization through deprotonation of the phosphine arms is blocked by methylation leads to ligand reactivity at the *para* carbon position with strong reductants. We reported two types of pyridine ring dearomatization, one via reduction in the *para*-position with a hydride source, and another through dimerization with the formation of a new C–C bond. DFT studies confirmed that the proposed transient, one-electron reduced (Me_4PNP^R)Ni–Me species are expected to demonstrate ligand-based radical, rather than the metal-based radical character previously observed in (Me_4PNP^R)Ni^{I}-X (X = Br, Cl) complexes, explaining their *para*-carbon based reactivity. These results suggest that if such ligand-based reactivity is to be avoided for further development of bulky, electron-rich PNP ligand, the *para* and possibly *meta* positions of the pyridine ring should be protected. The ligand based radical could possibly be stabilized by a ^{t}Bu moiety installed at the *para* carbon to avoid reactivity at the pyridine backbone. This may lead to a stable ligand based organic radical and a Ni^{II} center. These types of complexes may have interesting spectroscopic properties, and especially with other first-row metal centers, may be explored in metal-ligand spin coupling applications.

In addition, we showed that steric hindrance affects the outcome of Ni–Me and Ni–H complexes' reactivity in small molecule activation. In the case of significantly sterically hindered Me_4PNP^{tBu} ligand, we were able to obtain an unexpectedly stable Ni hydride complex that did not react with typical gaseous reagents and O_2 even after a prolonged reaction time. Reducing sterics by using the Me_4PNP^{iPr} ligand led to the observation of a transient superoxide species.

EXPERIMENTAL SECTION

All operations were performed using standard Schlenk or glovebox techniques under an N_2 atmosphere unless indicated otherwise. Unless otherwise indicated, all solvents and reagents were used as received. Non-deuterated solvents were taken from a solvent purification system (MBRAUN SPS). Acetone-d_6 was vacuum distilled over dried magnesium sulfate at low temperature. All other deuterated solvents were added to activated 3 Å molecular sieves. Methyl lithium 1M in diethyl ether and sodium tetraphenylborate were purchased from Kanto Chemicals. Sodium borohydride and lithium triethylborohydride were purchased from Tokyo Chemical Industry Co. Ltd. Copper(I) iodide was purchased from Nacalai Tesque Inc. Dimethylzinc 1M in heptane was purchased from Sigma. Potassium graphite was purchased from Strem Chemicals, Inc. Electrochemical grade tetrabutylammonium hexafluorophosphate ($^{n}Bu_4NPF_6$) from Fluka was used as the supporting electrolyte.

Complexes [(Me_4PNP^R)Ni^{II}Br]Br and [(Me_4PNP^R)Ni^{II}Br]B(Ar^F)$_4$ (R = ^{i}Pr, ^{t}Bu) were synthesized according to previously reported procedures.[77]

Cyclic voltammetry experiments were performed on an ALS CHI 660E electrochemical workstation. Electrochemical measurements were done under an N_2 atmosphere. Acetonitrile used for the solutions was dried through an MBRAUN SPS solvent system. A glassy carbon disk electrode (d = 1.6 mm) was used as working electrodes for cyclic voltammetry. A non-aqueous Ag-wire reference electrode assembly was filled with 0.01M $AgNO_3$ in 0.1 M $^{n}Bu_4NPF_6$/MeCN solution as a reference electrode. A Pt-wire was used as an auxiliary electrode. The reference electrodes were calibrated against $FeCp_2$ (Fc), where the Fc/Fc^{+} couple vs Ag/$AgNO_3$/MeCN non-aqueous reference is 102 V in 0.1 M $^{n}Bu_4NPF_6$/MeCN.

NMR spectra were recorded using JEOL ECZR-400 MHz or ECZR-600 MHz. Chemical shifts are reported in ppm (δ) and referenced internally to the residual solvent signals (^{1}H and

^{13}C: 7.26 and 77.16 ppm for $CDCl_3$; 2.05 and 29.84, 206.26 ppm for acetone-d_6; 1.94, 1.32 and 118.26 ppm for CD_3CN, and 7.16 and 128.08 ppm for C_6D_6). The signal abbreviations are as follows: d – doublet, t – triplet, v – virtual, q – quartet, br - broad, m – multiplet. X-band EPR spectra were recorded using an X-band JEOL JES-X330 instrument using a liquid nitrogen-cooled cryostat in 5 mm diameter quartz tubes. Fourier transform infrared (FT-IR) spectra were recorded for crystalline samples under an Ar atmosphere on Cary 630 with an attenuated-total-reflectance (ATR) module. Abbreviations are as follows: w – weak, m – medium, s – strong. UV-vis spectra were recorded on a Cary 60 UV-vis spectrophotometer between 200 and 1200 nm.

The X-ray diffraction data for the single crystals were collected on a Rigaku XtaLab PRO instrument (an ω-scan mode) with a PILATUS3 R 200K hybrid pixel array detector and a MicroMax^{TM}-003 microfocus X-ray tubes using Mo*Kα* (0.71073 Å) or Cu*Kα* (1.54184 Å) radiation at low temperature. Images were indexed and integrated using the *CrysAlis*^{Pro} data reduction package. Data were corrected for systematic errors and absorption using the *ABSPACK* module: Numerical absorption correction based on Gaussian integration over a multifaceted crystal model and empirical absorption correction based on spherical harmonics according to the point group symmetry using equivalent reflections. The *GRAL* module were used for analysis of systematic absences and space group determination. The XRD experiment for **[2]BPh$_4$** using Mo*Kα* radiation was performed on a Bruker D8 Venture diffractometer (a φ/ω-scan mode) equipped with a PHOTON II CPAD detector, an IμS 3.0 microfocus X-ray source, and an Oxford Cryostream LT device. Images were indexed and integrated using the *APEX3* data reduction package. Data were corrected for systematic errors and absorption by means of *SADABS* based on the Laue symmetry using equivalent reflections. *XPREP* was used for analysis of systematic absences and space group determination. All structures were solved by the direct methods using *SHELXT*[91] and refined by the full-matrix least-squares on F^2 using *SHELXL*.[92] Non-hydrogen atoms were refined anisotropically. The hydrogen atoms were inserted at the calculated positions and refined as riding atoms, except for hydrogens atoms on the nickel center, which were found using the difference Fourier maps. The positions of the hydrogen atoms of methyl groups were found using rotating group refinement with idealized tetrahedral angles. The disorder, if present, was resolved using free variables and reasonable restraints on geometry and anisotropic displacement parameters. Complexes **[4]B(Ar^F)$_4$** and **10** were resolved using the SQUEEZE routine of PLATON.[93]

[(Me$_4$PNP^{iPr})Ni^{II}Br]BPh$_4$, [1]BPh$_4$. Sodium tetraphenylborate ($NaBPh_4$) (36.4 mg, 0.106 mmol) was added to a solution of [(Me$_4$PNP^{iPr})Ni^{II}Br]Br (60.3 mg, 0.098 mmol) in THF and stirred at rt for 5 minutes. The solution was then evaporated and washed with diethyl ether to remove the remaining salt. The insoluble complex was collected on a short celite plug and washed with acetone and then evaporated to give a light orange solid (58 mg, 0.068 mmol, 70%). Yellow crystals suitable for X-ray diffraction were grown from a concentrated acetonitrile solution at -30 °C under an N_2. 1H NMR (400 MHz, $CDCl_3$): δ 1.16-1.22 (m, 12H, PCH-***C*H$_3$**), 1.51-1.55 (m overlap, 12H + 12 H, PCH-C***H*$_3$** + P-C(CH$_3$)$_2$C$_{py}$), 2.47-2.56 (m, 4H, P-C***H***CH$_3$), 6.57 (d, J_{HH} = 7.9 Hz, 2H, C$_{py}$-***H*$_{meta}$**), 6.88 (t, J_{HH} = 7.3 Hz, 4H, BC$_{Ar}$-***H*$_{para}$**), 7.02 (t, J_{HH} = 7.3 Hz, 8H, BC$_{Ar}$-***H*$_{meta}$**), 7.16 (t, J_{HH} = 8.0 Hz, 1H, C$_{py}$-***H*$_{para}$**), 7.42 (br m, 8H, BC$_{Ar}$-***H*$_{ortho}$**). ^{13}C{^{1}H} NMR (101 MHz, $CDCl_3$): δ 19.17 (PCH-***C*H$_3$**), 19.73 (PCH-***C*H$_3$**), 23.39 (vt, J_{PC} = 10.7 Hz, P***C***H-CH$_3$), 28.01 (P-C(***C*H$_3$**)$_2$C$_{py}$), 49.99 (vt, J_{PC} = 8.2 Hz, P-***C***(CH$_3$)C$_{py}$), 120.52 (vt, J_{PC} = 4.4 Hz, ***C*$_{py,meta}$**), 121.88 (B-***C*$_{Ar,para}$**), 125.67-125.74 (m, B-***C*$_{Ar,meta}$**), 136.43 (B-***C*$_{Ar,ortho}$**), 144.57 (***C*$_{py,para}$**), 164.27 (dd, J_{BC} = 49.2 Hz, B-***C*$_{Ar,ipso}$**), 172.38 (vt, J_{PC} = 7.1 Hz, ***C*$_{py,ortho}$**). ^{31}P{^{1}H} NMR (162 MHz, $CDCl_3$) 73.74. ATR-IR (cm^{-1}): 3045 (w), 2973 (w), 2874 (w), 1571 (w), 1457 (m), 1388 (w), 1369 (w). 1287 (w), 1244 (w), 1152 (w), 1100 (w), 1032 (w), 932 (w), 884 (w), 844 (w), 811 (w), 732 (m), 701 (s), 653 (m). UV-vis (THF, [1·10^{-4} M]), λ_{max}, nm (ε, L mol^{-1} cm^{-1}): 259 (21703), 276 (sh, 10429), 300 (6290), 345 (13442), 466 (1855). Anal. Calcd. For $C_{47}H_{63}NP_2NiBrB$: C, 66.15; H, 7.44; N, 1.64. Found: C, 65.92; H, 7.30; N, 2.27.

[(Me$_4$PNP^{tBu})Ni^{II}Br]BPh$_4$, [2]BPh$_4$. The same procedure to prepare **[1]BPh$_4$** was used to prepare **[2]BPh$_4$** starting from the previously reported [(Me$_4$PNP^{tBu})Ni^{II}Br]Br (50.0 mg, 0.075 mmol) and $NaBPh_4$ (26.8 mg, 0.078 mmol, 1.05 eq.) to afford a pink solid (59 mg, 0.065 mmol, 87%). Red crystals suitable for X-ray diffraction were grown from a concentrated acetone solution at r.t. ^{1}H NMR (400 MHz, CD_3CN): δ 1.42-1.45 (m, 18 H, Me of ^{t}Bu), 1.56-1.87 (br m, 18H, Me of ^{t}Bu), 1.90-1.96 (m overlapping with CD_3CN, 6H, P-C(C***H*$_3$**)$_2$C$_{py}$), 2.05-2.07 (m, 6H, P-C(CH$_3$)$_2$C$_{py}$), 6.85 (t, J_{HH} = 8.0 Hz, 4H, BC$_{Ar}$-***H*$_{para}$**), 7.00 (t, J_{HH} = 7.3 Hz, 8H, BC$_{Ar}$-***H*$_{meta}$**), 7.28 (t, J_{HH} = 6.2 Hz, 8H, BC$_{Ar}$-***H*$_{ortho}$**), 7.37 (d, J_{HH} = 8.1 Hz, 2H, C$_{py}$-***H*$_{meta}$**), 8.05 (t, J_{HH} = 8.0 Hz, 1H, C$_{py}$-***H*$_{para}$**). ^{13}C{^{1}H} NMR (101 MHz, CD_3CN): δ 24.88 (P-C(***C*H$_3$**)$_2$C$_{py}$), 32.15 (Me of ^{t}Bu), 32.94 (br, Me of ^{t}Bu), 36.05 (P-C(***C*H$_3$**)$_2$C$_{py}$), 40.11 (C$_{quat}$ of ^{t}Bu), 41.55 (vt, J_{PC} = 5.7 Hz, C$_{quat}$ of ^{t}Bu), 53.12 (vt, J_{PC} = 4.9 Hz, P-***C***(CH$_3$)$_2$C$_{py}$), 121.44 (***C*$_{py,meta}$**), 122.74 (B-***C*$_{Ar,para}$**), 126.54-126.62 (m, B-***C*$_{Ar,meta}$**), 136.99 (B-***C*$_{Ar,ortho}$**), 144.35 (***C*$_{py,para}$**), 164.74 (dd, J_{BC} = 49.3 Hz, B-***C*$_{Ar,ipso}$**), 174.01 (***C*$_{py,ortho}$**). ^{31}P{^{1}H} NMR (162 MHz, CD_3CN): δ 87.15. ATR-IR (cm^{-1}): 3051 (w), 3036 (w), 2998 (w), 2973 (w), 2936 (w), 2875 (w), 1599 (w), 1579 (w), 1563 (w), 1458 (m), 1427 (m), 1388 (w), 1367 (w), 1267 (w), 1243 (w), 1181 (w), 1146 (w), 1129 (w), 1100 (w), 1065 (w), 1047 (w) 1032 (m), 932 (w), 885 (w), 848 (w), 811 (w), 757 (m), 129 (s), 701 (s), 673 (m). UV-vis (THF, [1·10^{-4} M]), λ_{max}, nm (ε, L mol^{-1} cm^{-1}):. Anal. Calcd. For $C_{51}H_{71}NP_2NiBrB$: C, 67.35; H, 7.87; N, 1.54. Found: C, 66.72; H, 7.64; N, 1.56.

[(Me$_4$PNP^{iPr})Ni^{II}H]B(Ar^F)$_4$, [3]B(Ar^F)$_4$. Sodium tetrakis[3,5-bis(trifluoromethyl)phenyl]borate (NaB(Ar^F)$_4$) (14.7 mg, 0.017 mmol) was added to a THF solution of [(Me$_4$PNP^{iPr})Ni^{II}Br]Br (10.0 mg, 0.017 mmol) and stirred for 5 minutes. The mixture was then filtered over a short celite plug and sodium tetrahydroborate ($NaBH_4$) (6.3 mg, 0.17 mmol) was added followed by vigorous stirring for 4 hours to give a light-yellow solution. The solution was evaporated, and diethyl ether was added to dissolve the complex without dissolving the salts. The solution was filtered on a short celite plug and the solvent was evaporated to obtain a pale-yellow powder (23 mg, 0.017 mmol, 100 %). Yellow crystals suitable for X-ray diffraction were obtained by slow crystallization of a concentrated toluene solution of **[3]B(Ar^F)$_4$** at -30 °C under an N_2 ^{1}H NMR (400 MHz, acetone-d_6): δ -18.05 (t, J_{PH} = 54.8 Hz, 1H, Ni-***H***), 1.17-1.22 (m, 12H, PCH-C***H*$_3$**), 1.40-1.46 (m, 12H, PCH-C***H*$_3$**), 1.77-1.79 (m, 12H, PCH-C***H*$_3$**), 2.54-2.62 (m, 4H, PC***H***-CH$_3$), 7.62 (d, J_{HH} = 7.9 Hz, 2H, C$_{py}$-***H*$_{meta}$**), 7.67 (br s, BC$_{Ar}$-***H*$_{para}$**), 7.77-7.79 (m, 8H, BC$_{Ar}$-***H*$_{ortho}$**), 8.23 (tt, J_{HH} = 8.0, 1.3 Hz, 1H, C$_{py}$-***H*$_{para}$**). ^{13}C{^{1}H} NMR (101 MHz, acetone-d_6):

δ 20.68 (PCH-$\underline{\boldsymbol{C}}H_3$), 21.11 (PCH-$\underline{\boldsymbol{C}}H_3$), 24.20 (vt, J_{PC} = 11.5 Hz, P$\underline{\boldsymbol{C}}$H-CH$_3$), 26.15 27.89 (P-C($\underline{\boldsymbol{C}}H_3$)$_2C_{py}$), 51.27 (vt, J_{PC} = 7.6 Hz, P-$\underline{\boldsymbol{C}}$(CH$_3$)$_2C_{py}$), 118.37-118.53 (m, B-$\underline{\boldsymbol{C}}_{\underline{\boldsymbol{Ar,para}}}$), 120.52 (vt, J_{PC} = 4.6 Hz, $\underline{\boldsymbol{C}}_{\underline{\boldsymbol{py,meta}}}$), 125.36 (q, J_{CF} = 271.8 Hz, BC$_{Ar,meta}$-$\underline{\boldsymbol{C}}F_3$), 130.00 (qdd, J_{CF} = 30.5 Hz; J_{CB} = 5.7 Hz; J_{CF}= 2.7 Hz, B-$\underline{\boldsymbol{C}}_{\underline{\boldsymbol{Ar,meta}}}CF_3$), 135.52 (B-$\underline{\boldsymbol{C}}_{\underline{\boldsymbol{Ar,ortho}}}$), 143.16 ($\underline{\boldsymbol{C}}_{\underline{\boldsymbol{py,para}}}$), 162.58 (dd, J_{BC} = 49.9 Hz, B-$\underline{\boldsymbol{C}}_{\underline{\boldsymbol{Ar,ipso}}}$), 172.28 (vt, J_{PC} = 7.2 Hz, $\underline{\boldsymbol{C}}_{\underline{\boldsymbol{py,ortho}}}$). ^{31}P{^{1}H} NMR (162 MHz, acetone-d$_6$): δ 85.06 ^{19}F NMR (376 MHz, acetone-d$_6$): δ -63.14. ATR-IR (cm^{-1}): 2972 (w), 2940 (w), 1878 (w), 1925 (w), 1610 (w), 1564 (w), 1467 (w), 1389 (w), 1353 (s), 1270 (s), 1160 (s), 1118 (s), 1045 (m), 950 (w), 928 (w), 885 (m), 839 (m), 812 (w), 759 (w), 744 (w), 715 (m), 681 (m), 668 (s). UV-vis (THF, [1·10^{-4} M]), λ_{max}, nm (ε, L mol^{-1} cm^{-1}): 238 (35148), 242 (sh, 32044), 263 (sh, 18636), 269 (19436), .295 (7079), 381 (1688), 418 (sh, 827). Anal. Calcd. For $C_{55}H_{56}NP_2NiBF_{24}$: C, 50.10; H, 4.28; N, 1.06. Found: C, 49.15; H, 3.98; N, 1.04.

[(Me$_4$PNP^{iPr})Ni^{II}H]BPh$_4$, [3]BPh$_4$. To a solution of [(Me$_4$PNP^{iPr})Ni^{II}Br]Br (100.0 mg, 0.163 mmol) in dry THF under an N_2 atmosphere was added $NaBPh_4$ (58.5 mg, 0.171 mmol) and stirred for 5 minutes. The mixture was filtered over a short celite plug and to the solution is added $NaBH_4$ (61.6 mg, 1.63 mmol) and allowed to stir vigorously for 18 hours to give a dark solution. The solution is filtered on a short celite plug and the solvent is evaporated. Then, a minimum amount of acetonitrile or THF was added and the remaining salts were precipitated by adding pentane. The solids were filtered on a short celite pad and washed with a small amount of THF or acetonitrile to dissolve most of the complex. The solvent was evaporated to obtain a pale-yellow powder (114 mg, 0.147 mmol, 91%). Yellow crystals suitable for X-ray diffraction were obtained by slow crystallization of a concentrated THF solution of **[3]BPh$_4$** at -30 °C under an N_2. ^{1}H NMR (400 MHz, CD_3CN): δ -18.23 (t, J_{PH} = 54.9 Hz, 1H, Ni-$\underline{\boldsymbol{H}}$), 1.09-1.15 (m, 12H, PCH-C$\underline{\boldsymbol{H}}_{\underline{\boldsymbol{3}}}$), 1.34-1.40 (m, 12H, PCH-C$\underline{\boldsymbol{H}}_{\underline{\boldsymbol{3}}}$), 1.64-1.66 (m, 12H, P-C(C$\underline{\boldsymbol{H}}_{\underline{\boldsymbol{3}}}$)$_2C_{py}$), 2.42-2.51 (m, 4H, PC$\underline{\boldsymbol{H}}$-CH$_3$), 6.84 (tt, J_{HH} = 7.3 Hz, J_{PH} = 1.6 Hz, 4H, BC$_{Ar}$-$\underline{\boldsymbol{H}}_{\underline{\boldsymbol{para}}}$), 6.99 (t, J_{HH} = 7.4 Hz, 8H, BC$_{Ar}$-$\underline{\boldsymbol{H}}_{\underline{\boldsymbol{meta}}}$), 7.25-7.30 (m, 8H, BC$_{Ar}$-$\underline{\boldsymbol{H}}_{\underline{\boldsymbol{ortho}}}$), 7.38 (t, J_{HH} = 8.0 Hz, 2H C$_{py}$-$\underline{\boldsymbol{H}}_{\underline{\boldsymbol{meta}}}$), 8.02 (tt, J_{HH} = 8.0 Hz, J_{PH} = 1.3 Hz, 1H, C$_{py}$-$\underline{\boldsymbol{H}}_{\underline{\boldsymbol{para}}}$). ^{13}C{^{1}H} NMR (101 MHz, CD_3CN): δ .20.68 (PCH-$\underline{\boldsymbol{C}}H_3$), 21.12 (PCH-$\underline{\boldsymbol{C}}H_3$), 24.21 (vt, J_{PC} = 11.5 Hz, P$\underline{\boldsymbol{C}}$H-CH$_3$), 27.94 (P-C($\underline{\boldsymbol{C}}H_3$)C$_{py}$), 51.21 (vt, J_{PC} = 7.6 Hz, P-$\underline{\boldsymbol{C}}$(CH$_3$)$_2C_{py}$), 120.39 (vt, J_{PC} = 3.8 Hz, $\underline{\boldsymbol{C}}_{\underline{\boldsymbol{py,meta}}}$), 122.76 (B-$\underline{\boldsymbol{C}}_{\underline{\boldsymbol{Ar,para}}}$), 126.58 (vdd, J_{BC} = 4.8 Hz, 2.4 Hz, B-$\underline{\boldsymbol{C}}_{\underline{\boldsymbol{Ar,meta}}}$), 136.73 (B-$\underline{\boldsymbol{C}}_{\underline{\boldsymbol{Ar,ortho}}}$), 142.90 ($\underline{\boldsymbol{C}}_{\underline{\boldsymbol{py,para}}}$), 164.79 (dd, J_{BC} = 98.4 Hz, 49.2 Hz, B-$\underline{\boldsymbol{C}}_{\underline{\boldsymbol{Ar,ipso}}}$), 172.22 (vt, J_{PC} = 7.2 Hz, $\underline{\boldsymbol{C}}_{\underline{\boldsymbol{py,ortho}}}$). ^{31}P{^{1}H} NMR (162 MHz, CD_3CN): δ 84.91. ATR-IR (cm^{-1}):3055 (w), 3029 (w), 2893 (w), 2971 (w), 2958 (w), 2931 (w), 2869 (w), 2290 (w), 1579 (w), 1563 (w), 1455 (w), 1427 (w), 1384 (w), 1367 (w), 1256 (w), 1240 (w), 1186 (w), 1151 (w), 1129 (w), 1116 (w), 1098 (w), 1068 (w), 1032 (w), 932 (w), 885 (w), 842 (w), 813 (w), 745 (m), 731 (m), 701 (s), 663 (m). UV-vis (THF, [1·10^{-4} M]), λ_{max}, nm (ε, L mol^{-1} cm^{-1}): 260 (sh, 14681), 266 (sh,1 2426), 275 (8605), 300 (4526), 340 (4702), 369 (sh ,3445). Anal. Calcd. For $C_{47}H_{64}NP_2NiBrB$: C, 72.89; H, 8.33; N, 1.81. Found: C, 72.04; H, 8.06; N, 2.24.

[(Me$_4$PNP^{tBu})Pyridine)Ni^{II}H][B(Ar^F)$_4$], [4]B(Ar^F)$_4$. The same procedure to prepare **[3]B(Ar^F)$_4$** was used to prepare **[4]B(Ar^F)$_4$** using [(Me$_4$PNP^{tBu})Ni^{II}Br]Br (10.0 mg, 0.015 mmol), NaB(Ar^F)$_4$ (13.2 mg, 0.0149 mmol) and $NaBH_4$ (5.6 mg, 0.15 mmol). A pale-yellow solid was obtained (22 mg, 0.016 mmol, 100%). Yellow crystals suitable for X-ray diffraction were grown from a concentrated anhydrous THF solution of **[4]B(Ar^F)$_4$** at -30 °C under an N_2. ^{1}H NMR (400 MHz, acetone-d$_6$): δ -17.95 (t, J_{HP} = 50.4 Hz, 1H, Ni-$\underline{\boldsymbol{H}}$), 1.46-1.49 (m, 36H, Me of ^{t}Bu), 1.95-1.97 (m, 12H, P-C(C$\underline{\boldsymbol{H}}_{\underline{\boldsymbol{3}}}$)C$_{py}$), 7.58 (d, J_{HH} = 8.1 Hz, 2H, C$_{py}$-$\underline{\boldsymbol{H}}_{\underline{\boldsymbol{meta}}}$), 7.67 (br s, 4H, BC$_{Ar}$-$\underline{\boldsymbol{H}}_{\underline{\boldsymbol{para}}}$), 7.76-7.80 (m, 8H, BC$_{Ar}$-$\underline{\boldsymbol{H}}_{\underline{\boldsymbol{ortho}}}$), 8.22 (t, J_{HH} = 8.1 Hz, 1H, C$_{py}$-$\underline{\boldsymbol{H}}_{\underline{\boldsymbol{para}}}$). ^{13}C{^{1}H} NMR (101 MHz, acetone-d$_6$): δ 29.27-30.42 (overlap acetone-d$_6$ and P-C($\underline{\boldsymbol{C}}H_3$)$_2C_{py}$), 31.65 (Me of ^{t}Bu), 38.00 (vt, J_{PC} = 7.0 Hz, C$_{quat}$ of ^{t}Bu), 54.41 (vt, J_{PC} = 3.9 Hz, P-$\underline{\boldsymbol{C}}$(CH$_3$)$_2C_{py}$), 118.38-118.53 (m, B-$\underline{\boldsymbol{C}}_{\underline{\boldsymbol{Ar,para}}}$), 119.90 (vt, J_{PC} = 4.2 Hz, $\underline{\boldsymbol{C}}_{\underline{\boldsymbol{py,meta}}}$), 125.36 (q, J_{CF} = 271.9 Hz, BC$_{Ar,meta}$-$\underline{\boldsymbol{C}}F_3$), 130.00 (qdd, J_{CF} = 31.6 Hz; J_{CB} = 5.3 Hz; J_{CF}= 2.6 Hz, B-$\underline{\boldsymbol{C}}_{\underline{\boldsymbol{Ar,meta}}}CF_3$), 135.52 (B-$\underline{\boldsymbol{C}}_{\underline{\boldsymbol{Ar,ortho}}}$), 143.31 ($\underline{\boldsymbol{C}}_{\underline{\boldsymbol{py,para}}}$), 162.58 (dd, J_{BC} = 49.9 Hz, B-$\underline{\boldsymbol{C}}_{\underline{\boldsymbol{Ar,ipso}}}$), 172.68 (vt, J_{PC} = 7.0 Hz, $\underline{\boldsymbol{C}}_{\underline{\boldsymbol{py,ortho}}}$). ^{31}P{^{1}H} NMR (162 MHz, acetone-d$_6$): δ 108.22. ^{19}F NMR (376 MHz, acetone-d$_6$): δ -63.12. ATR-IR (cm^{-1}): 3003 (w), 2965 (w), 2906 (w), 1919 (w), 1606 (w), 1564 (w), 1467 (w), 1392 (w), 1353 (m), 1270 (m), 1170 (m), 1125 (s), 1019 (w), 926 (w), 888 (m), 835 (w), 809 (w), 711 (m), 674 (m). UV-vis (THF, [1·10^{-4} M]), λ_{max}, nm (ε, L mol^{-1} cm^{-1}): 274 (14904), 356 (6089), 477 (278). ESI-HRMS (*m/z*) calculated for [$C_{27}H_{52}NNiP_2$]$^+$ = 510.2923, and for [$C_{32}H_{12}BF_{24}$]$^-$ = 863.0649. Found for [$C_{27}H_{52}NNiP_2$]$^+$ = 510.2912, and for [$C_{32}H_{12}BF_{24}$]$^-$ = 863.0632. Anal. Calcd. For $C_{59}H_{64}NP_2NiBF_{24}$: C, 51.55; H, 4.69; N, 1.02. Found: C, 51.30; H, 4.81; N, 1.15.

[(Me$_4$PNP^{tBu})Ni^{II}H]BPh$_4$, [4]BPh$_4$. The same procedure to prepare **[3]BPh$_4$** was used to prepare **[4]BPh$_4$** using [(Me$_4$PNP^{tBu})Ni^{II}Br]Br (50.0 mg, 0.075 mmol), $NaBPh_4$ (26.8 mg, 0.078 mmol), and $NaBH_4$ (28.2 mg, 0.75 mmol) to afford a white solid (60 mg, 0.072 mmol, 97%). Crystals suitable for X-ray diffraction were obtained by slow crystallization of a concentrated THF solution of **[4]BPh$_4$** at -30 °C under an N_2. ^{1}H NMR (400 MHz, $CDCl_3$): δ -18.13 (t, J_{HP} = 50.5 Hz, 1H, Ni-$\underline{\boldsymbol{H}}$), 1.36-1.40 (m, 36H, Me of ^{t}Bu), 1.68-1.71 (m, 12H, C$_{quat}$ of ^{t}Bu), 6.79 (d, J_{HH} = 8.0 Hz, 2H, C$_{py}$-$\underline{\boldsymbol{H}}_{\underline{\boldsymbol{meta}}}$), 6.89 (t, J_{HH} = 7.1 Hz, 4H, BC$_{Ar}$-$\underline{\boldsymbol{H}}_{\underline{\boldsymbol{para}}}$), 7.03 (t, J_{HH} = 7.3 Hz, 8H, BC$_{Ar}$-$\underline{\boldsymbol{H}}_{\underline{\boldsymbol{meta}}}$), 7.39 (t, J_{HH} = 8.1 Hz, 1H (overlaps), C$_{py}$-$\underline{\boldsymbol{H}}_{\underline{\boldsymbol{para}}}$), 7.41-7.44 (m, 8H (overlaps), BC$_{Ar}$-$\underline{\boldsymbol{H}}_{\underline{\boldsymbol{ortho}}}$). ^{13}C{^{1}H} NMR (101 MHz, $CDCl_3$): δ 29.98 (br, P-C($\underline{\boldsymbol{C}}H_3$)$_2C_{py}$), 31.54 (Me of ^{t}Bu), 37.48 (vt, J_{PC} = 6.7 Hz, C$_{quat}$ of ^{t}Bu), 53.48 (vt, J_{PC} = 3.8 Hz, P-$\underline{\boldsymbol{C}}$(CH$_3$)$_2C_{py}$), 118.69 (vt, J_{PC} = 4.0 Hz, $\underline{\boldsymbol{C}}_{\underline{\boldsymbol{py,meta}}}$), 121.78 (B-$\underline{\boldsymbol{C}}_{\underline{\boldsymbol{Ar,para}}}$), 125.61-125.69 (m, B-$\underline{\boldsymbol{C}}_{\underline{\boldsymbol{Ar,meta}}}$), 136.48 (B-$\underline{\boldsymbol{C}}_{\underline{\boldsymbol{Ar,ortho}}}$), 143.21 ($\underline{\boldsymbol{C}}_{\underline{\boldsymbol{py,para}}}$), 164.39 (dd, J_{BC} = 49.4 Hz, B-$\underline{\boldsymbol{C}}_{\underline{\boldsymbol{Ar,ipso}}}$), 171.08 (vt, J_{PC} = 7.1 Hz, $\underline{\boldsymbol{C}}_{\underline{\boldsymbol{py,ortho}}}$). ^{31}P{^{1}H} NMR (162 MHz, $CDCl_3$): δ 107.78. ATR-IR (cm^{-1}): 3057 (w), 2995 (w), 2971 (w), 2901 (w), 1896 (w), 1579 (w), 1560 (w), 1478 (w), 1456 (W), 1427 (w), 1393 (w), 1366 (w), 1255 (w), 1176 (w), 1154 (w), 1128 (w), 1105 (w), 1069 (w), 1031 (w), 994 (w), 822 (w), 846 (w), 812 (w), 743 (s), 711 (s). UV-vis (THF, [1·10^{-4} M]), λ_{max}, nm (ε, L mol^{-1} cm^{-1}): 260 (sh, 11568), 267 (sh, 9859), 275 (6506), 289 (4217), 341 (4154), 372 (sh, 2673). ESI-HRMS (*m/z*) calculated for [$C_{27}H_{52}NNiP_2$]$^+$ = 510.2923, and for [$C_{24}H_{20}B$]$^-$ = 319.1653. Found for [$C_{27}H_{52}NNiP_2$]$^+$ = 510.2905, and for [$C_{24}H_{20}B$]$^-$ = 319.1652. Despite multiple attempts, satisfactory elemental analysis could not be obtained. However, the sample was pure from other organometallic impurities according to ^{1}H, ^{13}C and ^{31}P NMR (See Supporting Information)

[(Me$_4$PNP^{iPr})Ni^{II}Me]B(Ar^F)$_4$, [5]B(Ar^F)$_4$.

Method 1. NaB(Ar^F)$_4$ (88.0 mg, 0.099 mmol) was added to a 20 mL vial containing a solution of [(Me$_4$PNP^{iPr})Ni^{II}Br]Br (60.0 mg, 0.099 mmol) in THF (10 mL). After stirring for 5 minutes, MeLi (1.17 M in THF, 85 µL, 0.099 mmol) was add-

ed to the solution, which was stirred at r.t. for an hour. The solution was then evaporated, washed with hexanes, filtered through a short celite pad and evaporated to afford a yellowish powder (106 mg, 0.079 mmol, 80%). Yellow crystals suitable for X-ray diffraction were obtained by slow crystallization in THF at -30°C.

Method 2. $NaB(Ar^F)_4$ (66.0 mg, 0.075 mmol) was added to a 20 mL vial containing a solution of $[(Me_4PNP^{iPr})Ni^{II}Br]Br$ (45.0 mg, 0.0745 mmol) in THF (10 mL) and stirred for 5 minutes. In another 5 mL vial a homogeneous solution of copper(I) iodide (14.1 mg, 0.075 mmol) in diethyl ether (2 mL) was added to a cold solution of MeLi (1.17 M in THF, 127 uL, 0.149 mmol). A yellow solid, lithium dimethylcuprate, precipitates instantly and the whole solution in the 5 mL vial was transferred quickly to the 20 mL vial, followed by a rapid color change to black. The solution was immediately filtered through a short celite pad, evaporated and washed with hexanes, filtered on celite and evaporated to afford a yellowish powder (92 mg, 0.069 mmol, 93%).

Method 3. $NaB(Ar^F)_4$ (72.1 mg, 0.0814 mmol) was added to a 20 mL vial containing a solution of $[(Me_4PNP^{iPr})Ni^{II}Br]Br$ (50.0 mg, 0.0814 mmol) in THF (10 mL). After stirring for 5 minutes, $ZnMe_2$ (1.0 M in hexanes, 163 uL, 0.163, mmol, 2.0 eq.) was added to the reaction, which was stirred at r.t. for 2 hours before gradually turning black. The solution filtered on through a short celite pad, evaporated, washed with diethyl ether, and dried under vacuum to afford a yellowish powder (85 mg, 0.064 mmol, 79%). ^{1}H NMR (400 MHz, acetone-d_6): δ -0.16 (t, J_{PH} = 8.5 Hz, 3 H, Ni-C***H***$_3$), 1.21-1.26 (m, 12H, PCH-C***H***$_3$), 1.43-1.49 (m, 12H, PCH-***CH***$_3$), 1.80-1.83 (m, 12H, P-C(C***H***$_3$)$_2$C$_{py}$), 2.59-2.68 (m, 4H, PC***H***-CH$_3$), 7.57 (d, J_{HH} = 7.3 Hz, 2H, C$_{py}$-***H***$_{meta}$), 7.66 (br s, 4H, BC$_{Ar}$-***H***$_{para}$), 7.77-7.79 (br m, 8H, BC$_{Ar}$-***H***$_{ortho}$), 8.18 (t, J_{HH} = 8.0 Hz, 1H, C$_{py}$-***H***$_{para}$). ^{13}C{^{1}H} NMR (101 MHz, acetone-d_6): δ -16.33 (t, J_{PC} = 21.6 Hz, Ni-***C***H$_3$), 19.31 (PCH-***C***H$_3$), 19.91 (P***C***H-CH$_3$), 23.06 (vt, J_{PC} = 10.1 Hz, P***C***H-CH$_3$), 28.21 (P-C(***C***H$_3$)$_2$C$_{py}$), 50.55 (vt, J_{PC} = 8.1 Hz, P-***C***(CH$_3$)$_2$C$_{py}$), 118.37-118.53 (m, B-***C***$_{Ar,para}$), 120.39 (vt, J_{PC} = 4.2 Hz, ***C***$_{py,meta}$), 125.36 (q, J_{CF} = 271.6 Hz, BC$_{Ar,meta}$-***C***F$_3$), 129.99 (qdd, J_{CF} = 31.7 Hz; J_{CB} = 5.0 Hz; J_{CF}= 2.4 Hz, B-***C***$_{Ar,meta}$CF$_3$), 135.52 (B-***C***$_{Ar,ortho}$), 142.91 (***C***$_{py,para}$), 162.57 (dd, J_{BC} = 50.0 Hz, B-***C***$_{Ar,ipso}$), 171.95 (vt, J_{PC} = 6.9 Hz, ***C***$_{py,ortho}$). ^{31}P{^{1}H} NMR (162 MHz, acetone-d_6): δ 70.15. ^{19}F NMR (376 MHz, acetone-d_6): δ -63.14. ATR-IR (cm^{-1}): 2969 (w) 2879 (w), 1605 (w), 1567 (w), 1464 (w), 1391 (w), 1352 (m), 1271 (s), 1157 (m), 1118 (s), 1038 (w), 928 (w), 886 (m), 835 (w), 815 (w), 751 (m), 711 (m), 674 (m). UV-vis (THF, [1·10^{-4} M]), λ_{max}, nm (ε, L mol^{-1} cm^{-1}): 274 (14904), 356 (6089). ESI-HRMS (*m/z*) calculated for $[C_{24}H_{46}NNiP_2]^+$ = 468.2453, and for $[C_{32}H_{12}BF_{24}]^-$ = 863.0643. Found for $[C_{24}H_{46}NNiP_2]^+$ = 468.2443 and for $[C_{32}H_{12}BF_{24}]^-$ = 863.0661. Despite multiple attempts, satisfactory elemental analysis could not be obtained due to traces of solvent. However, the sample was pure from organic/organometallic impurities according to ^{1}H, ^{13}C and ^{31}P NMR (See Supporting Information).

$[(Me_4PNP^{iPr})Ni^{II}Me]BPh_4$, [5]$BPh_4$. This complex was prepared following **Method 3** described for the preparation of **[5]B(Ar^F)$_4$** using $[(Me_4PNP^{iPr})Ni^{II}Br]Br$ (50.0 mg, 0.0814 mmol), $NaBPh_4$ (27.8 mg, 0.0814 mmol), and $ZnMe_2$ (1.0 M in hexanes, 163 uL, 0.163 mmol). Washing was done with hexanes then the solid was solubilized with a minimal amount of THF or acetonitrile and evaporated to afford an off-white powder (56 mg, 0.071 mmol, 87%). Pale yellow crystals suitable for X-ray diffraction were obtained by slow crystallization of a concentrated solution of **[5]BPh$_4$** in THF at -30 °C under an N_2 atmosphere. ^{1}H NMR (600 MHz, CD_3CN): δ -0.23 (t, J_{PH} = 8.3 Hz, 3H Ni-C***H***$_3$), 1.13-1.16 (m, 12H, PCH-C***H***$_3$), 1.38-1.41 (m, 12H, PCH-C***H***$_3$), 1.68-1.70 (m, 12H, P-C(C***H***$_3$)$_2$C$_{py}$), 2.48-2.57 (m, 4H, PC***H***-CH$_3$), 6.84 (t, J_{HH} = 7.1 Hz, 4H, BC$_{Ar}$-***H***$_{para}$), 6.99 (t, J_{HH} = 7.3 Hz, 8H, BC$_{Ar}$-***H***$_{meta}$), 7.27-7.28 (m, 8H, BC$_{Ar}$-***H***$_{ortho}$), 7.33 (d, J_{HH} = 8.1 Hz, 8H, C$_{py}$-***H***$_{meta}$), 7.98 (t, J_{HH} = 8.0 Hz, 1H, C$_{py}$-***H***$_{para}$). ^{13}C{^{1}H} NMR (151 MHz, CD_3CN): δ -16.49 (t, J_{PC} = 21.8 Hz, Ni-***C***H$_3$), 19.35 (PCH-***C***H$_3$), 19.93 (PCH-***C***H$_3$), 23.09 (vt, J_{PC} = 10.1 Hz, P***C***H-CH$_3$), 28.27 (s, P-C(***C***H$_3$)$_2$C$_{py}$), 50.51 (vt, J_{PC} = 8.0 Hz, P-***C***(CH$_3$)$_2$C$_{py}$), 120.27 (vt, J_{PC} = 4.0 Hz, ***C***$_{py,meta}$), 122.75 (B-***C***$_{Ar,para}$), 126.5-126.6 (m, B-***C***$_{Ar,meta}$), 136.73 (B-***C***$_{Ar,ortho}$), 142.67 (***C***$_{py,para}$), 164.79 (dd, J_{BC} = 49.2 Hz, B-***C***$_{Ar,ipso}$), 171.88 (vt, J_{PC} = 7.2 H$_z$, ***C***$_{py,ortho}$). ^{31}P{^{1}H} NMR (243 MHz, CD_3CN): δ 70.09. ATR-IR (cm^{-1}): 3042 (w), 2972 (w), 2878(w), 1709 (w), 1591 (w), 1570 (w), 1455 (w), 1389 (w), 1361 (w), 1266 (w), 1247 (w), 1153 (w), 1123(w), 1100 (w), 1072 (w), 1028 (w), 931 (w), 885 (w), 841 (w), 814 (w), 733 (m), 698 (s), 661 (m). UV-vis (THF, [1·10^{-4} M]), λ_{max}, nm (ε, L mol^{-1} cm^{-1}): 267 (sh, 8014), 274 (sh, 5368), 291 (2999), 349 (3399), 383 (sh, 1861). ESI-HRMS (*m/z*) calculated for $[C_{24}H_{46}NNiP_2]^+$ = 468.2453, and for $[C_{24}H_{20}B]^-$ = 319.1653. Found for $[C_{24}H_{46}NNiP_2]^+$ = 468.2442, and for $[C_{24}H_{20}B]^-$ = 319.1652 Anal. Calcd. For $C_{48}H_{66}NP_2NiB$: C, 73.12; H, 8.44; N, 1.78. Found: C, 72.81; H, 8.12; N, 1.90.

$[(Me_4PNP^{tBu})Ni^{II}Me]B(Ar^F)_4$, [6]B(Ar^F)$_4$. This complex was prepared using the **Method 3** described for the preparation of **[5]B(Ar^F)$_4$** using $[(Me_4PNP^{tBu})Ni^{II}Br]Br$ (50.0 mg, 0.0746 mmol), $NaB(Ar^F)_4$ (66.1 mg, 0.0746 mmol), and $ZnMe_2$ (1.0 M in hexanes. 149 uL, 0.149 mmol), giving a yellowish powder (100 mg, 0.072 mmol, 97%). Orange crystals suitable for X-ray diffraction studies were obtained by vapor diffusion of diethyl ether into a concentrated benzene solution of **[6]B(Ar^F)$_4$** at RT. ^{1}H NMR (400 MHz, CD_3CN): δ 0.06 (t, J_{HP} = 8.2 Hz, 3H, Ni-C***H***$_3$), 1.24-1.35 (m, 18H, Me of ^{t}Bu), 1.62-1.75 (m, 18H, Me of ^{t}Bu), 1.81-1.88 (m, 6H, P-C(C***H***$_3$)$_2$C$_{py}$), 1.96-2.01 (m, 6H, P-C(C***H***$_3$)$_2$C$_{py}$), 7.34 (d, J_{HH} = 8.1 Hz, 2H, C$_{py}$-***H***$_{meta}$), 7.65-7.68 (m, 4H, BC$_{Ar}$-***H***$_{para}$), 7.68-7.72 (m, 8H, BC$_{Ar}$-***H***$_{ortho}$), 7.99 (t, J_{HH} = 8.2 Hz, 1H, C$_{py}$-***H***$_{para}$). ^{13}C{^{1}H} NMR (101 MHz, CD_3CN): δ -20.04 (weak signal, Ni-***C***H$_3$), 24.54 (P-C(***C***H$_3$)$_2$C$_{py}$), 31.97 (Me of ^{t}Bu), 32.56 (br, Me of ^{t}Bu), 36.07 (P-C(***C***H$_3$)$_2$C$_{py}$), 38.53 (C$_{quat}$ of ^{t}Bu), 39.26 (C$_{quat}$ of ^{t}Bu), 52.56 (vt, J_{PC} = 4.7 Hz, P-***C***(CH$_3$)$_2$C$_{py}$), 120.00 (***C***$_{py,meta}$), 125.42 (q, J_{CF} = 272.5 Hz, BC$_{Ar,meta}$-***C***F$_3$), 129.90 (qdd, J_{CF} = 31.6 Hz; J_{CB} = 5.9 Hz; J_{CF}= 2.9 Hz, B-***C***$_{Ar,meta}$CF$_3$), 135.64 (B-***C***$_{Ar,ortho}$), 142.78 (***C***$_{py,para}$), 161.86-163.34 (m, B-***C***$_{Ar,ipso}$), 172.04 (***C***$_{py,ortho}$). ^{31}P{^{1}H} NMR (162 MHz, CD_3CN): δ 86.05. ^{19}F NMR (471 MHz, $CDCl_3$): δ -63.14. ATR-IR (cm^{-1}): 2972 (w), 2874 (w), 1605 (w), 1460 (w), 1392 (w), 1352 (m), 1271 (s), 1165 (m), 1124 (s), 1026 (m), 1014 (m), 927 (w), 887 (m), 834 (w), 807 (w), 40 (w), 709 (m), 674 (m). UV-vis (THF, [1·10^{-4} M]), λ_{max}, nm (ε, L mol^{-1} cm^{-1}): 269 (sh, 13790), 279 (sh, 9966), 358 (3957), 455 (544). ESI-HRMS (*m/z*) calculated for $[C_{28}H_{54}NNiP_2]^+$ = 524.3079, and for $[C_{32}H_{12}BF_{24}]^-$ = 863.0643. Found for $[C_{28}H_{54}NNiP_2]^+$ = 524.3072 and for $[C_{32}H_{12}BF_{24}]^-$ = 863.0654. Despite multiple attempts, satisfactory elemental analysis could not be obtained due to traces of solvent. However, the sample was pure from organometallic impurities according to ^{1}H, ^{13}C and ^{31}P NMR (See Supporting Information).

[(Me$_4$PNP^{tBu})Ni^{II}Me]BPh$_4$, [6]BPh$_4$. This complex was prepared following **method 3** described for the preparation of **[5]B(Ar^F)$_4$** using [(Me$_4$PNP^{tBu})Ni^{II}Br][Br] (50.0 mg, 0.0746 mmol), NaBPh$_4$ (25.5 mg, 0.0746 mmol), and ZnMe$_2$ (1.0 M in hexanes, 149 uL, 0.149 mmol). Washing was done with hexanes, then the solid was solubilized with a minimal amount of THF or acetonitrile and evaporated to afford a light yellow powder (51 mg, 0.062 mmol, 81%). Yellow crystals suitable for X-ray diffraction were obtained by slow crystallization of a concentrated solution of **[6]BPh$_4$** in THF at -30 °C under an N_2 atmosphere. ^{1}H NMR (600 MHz, CD_3CN): δ 0.06 (t, J_{PH} = 8.3 Hz, 3H, Ni-C***H*$_3$**), 1.23-1.38 (br s, 18H, Me of ^{t}Bu), 1.62-1.74 (br s, 18H, Me of ^{t}Bu), 1.79-1.88 (br s, 6H. P-C(C***H*$_3$**)$_2$C$_{py}$), 1.95-2.00 (br s, 6H), 6.84 (t, J_{HH} = 7.6 Hz, 4H, BC$_{Ar}$-***H*$_{para}$**), 6.99 (t, J_{HH} = 7.7 Hz, 8H, BC$_{Ar}$-***H*$_{meta}$**), 7.23-7.31 (br m, 8H, BC$_{Ar}$-***H*$_{ortho}$**), 7.34 (d, J_{HH} = 8.9 Hz, 2H, C$_{py}$-***H*$_{meta}$**), 7.98 (t, J_{HH} = 8.1 Hz, 1H, C$_{py}$-***H*$_{para}$**). ^{13}C{^{1}H} NMR (151 MHz, CD_3CN): δ -20.06 (weak signal, Ni-***C***H$_3$), 24.58 (P-C(***C***H$_3$)C$_{py}$), 32.02 (Me of ^{t}Bu), 32.57 (br, Me of ^{t}Bu), 36.09 (P-C(***C***H$_3$)$_2$C$_{py}$), 38.54 (C$_{quat}$ of ^{t}Bu), 39.29 (C$_{quat}$ of ^{t}Bu), 52.59 (P-***C***(CH$_3$)$_2$C$_{py}$), 120.03 (***C*$_{py,meta}$**), 122.76 (B-***C*$_{Ar,para}$**), 126.57 (B-***C*$_{Ar,meta}$**), 136.73 (B-***C*$_{Ar,ortho}$**), 142.85 (***C*$_{py,para}$**), 164.79 (q, J_{BC} = 49.5 Hz, B-***C*$_{Ar,ipso}$**), 172.03 (***C*$_{py,ortho}$**). ^{31}P{^{1}H} NMR (243 MHz, CD_3CN): δ 86.10. ATR-IR (cm^{-1}): 3032 (w), 2976 (w), 2897 (w), 2318 (w), 2288 (w), 1706 (w), 1573 (w), 1453 (w), 1361 (w), 1256 (w), 1167 (w), 1065 (w), 1026 (w), 925 (w), 841 (w), 809 (w), 734 (m), 701 (s). UV-vis (THF, [1·10^{-4} M]), λ_{max}, nm (ε, L mol^{-1} cm^{-1}): 274 (14904), 356 (6089). ESI-HRMS (*m/z*) calculated for $[C_{28}H_{54}NNiP_2]^+$ = 524.3079, and for $[C_{24}H_{20}B]^-$ = 319.1653. Found for $[C_{28}H_{54}NNiP_2]^+$ = 524.3043 and for $[C_{24}H_{20}B]^-$ =319.1323 Despite multiple attempts, satisfactory elemental analysis could not be obtained due to traces of solvent that could not be fully removed under vacuum.

(Me$_4$PNP^{iPr}·H)Ni^{II}Br, 7. To a solution of **[1]BPh$_4$** (50 mg, 0.058 mmol) in THF, LiBEt$_3$H (1.0 M in THF, 58 μL, 0.058 mmol, 1 eq) was added and the solution instantly changed color to green. The solution was concentrated to 1 mL under reduced pressure, then diethyl ether was added and the solid was removed by filtration on a short celite plug. The diethyl ether solution was then evaporated under reduced pressure to obtain a green powder (27 mg, 0.050 mmol, 87%). Green crystals suitable for X-ray diffraction were grown from layering of diethyl ether on a concentrated benzene solution of **7** at rt under an N_2. ^{1}H NMR (400 MHz, C_6D_6): δ 1.28-1.31 (m, 12H, P-C(C***H*$_3$**)$_2$C$_{py}$), 1.34-1.39 (m, 12H, PCH-C***H*$_3$**), 1.55-1.60 (m, 12H, PCH-C***H*$_3$**), 2.23-2.32 (m, 4H, PC***H***-CH$_3$), 2.95 (m, 2H, C$_{hydropy}$-***H*$_{para}$**), 4.23 (m, 2H, C$_{hydropy}$-***H*$_{meta}$**). ^{13}C{^{1}H} NMR (101 MHz, C_6D_6): δ 18.45 (PCH-***C***H$_3$), 20.25 (PCH-***C***H$_3$), 23.68 (vt, J_{PC} = 9.1 Hz, P***C***H-CH$_3$), 24.94 (***C*$_{hydropy,para}$**), 26.11 (P-C(***C***H$_3$)$_2$C$_{hydropy,ortho}$), 43.78 (vt, J_{PC}= 8.8 Hz, P-***C***(CH$_3$)$_2$C$_{hydropy,ortho}$), 91.35 (vt, J_{PC} = 6.6 Hz, ***C*$_{hydropy,meta}$**), 160.99 (vt, J_{PC} = 6.9 Hz, ***C*$_{hydropy,ortho}$**). ^{31}P{^{1}H} NMR (162 MHz, C_6D_6): δ 62.48. ATR-IR (cm^{-1}): 2958 (w), 2919 (w), 2867 (w), 2838 (w), 2746 (w), 2163 (w), 1962 (w), 1646 (w), 1600 (w), 1459 (w), 1380 (w), 1333 (w), 1298 (w), 1240 (w), 1205 (w), 1160 (w), 1125 (w), 1095 (w), 1027 (m), 989 (w), 932 (w), 885 (w), 804 (w), 804 (w), 752 (w), 720 (w), 695 (m), 657 (s). UV-vis (CH_2Cl_2, [0.5·10^{-4} M]), λ_{max}, nm (ε, L mol^{-1} cm^{-1}): 233 (32419), 259 (sh, 16945), 286 (8256), 322 (13815), 352 (sh, 7213), 433 (2105), 656 (1001). ESI-HRMS (*m/z*) calculated for $[C_{23}H_{44}NBrNiP_2]^+$ = 532.1402. Found for $[C_{23}H_{44}NBrNiP_2]^+$ = 532.1390. Despite multiple attempts, satisfactory elemental analysis could not be obtained.

(Me$_4$PNP^{tBu}·H)Ni^{II}Br, 8. To a solution of **[2]BPh$_4$** (16.0 mg, 0.0176 mmol) in THF, LiBEt$_3$H (1.0 M in THF, 14 μL, 0.014 mmol, 0.8 eq) was added and the solution instantly changed color to green. The solution was concentrated to a volume of less than 1 mL, and 5 mL of diethyl ether was added. The precipitate was filtered on a short celite pad, and the remaining diethyl ether solution was then evaporated under reduced pressure to afford a green powder (8 mg, 0.014 mmol, 77%). Green crystals suitable for X-ray diffraction were grown from the reaction of 1 equivalent of LiBEt$_3$H via layering of diethyl ether into a concentrated benzene solution of **8** at rt under an N_2. Crystals of **8** are disordered with a hydride species, which is not observed in **7**. ^{1}H NMR (400 MHz, C_6D_6): δ 1.32-1.37 (m, 6H, P-C(C***H*$_3$**)$_2$C$_{hydropy}$), 1.50-1.92 (m (overlap), 6H + 36H, P-C(C***H*$_3$**)$_2$C$_{py}$ + Me of ^{t}Bu), 2.73-2.88 (m, 2H, C$_{hydropy}$-***H*$_{para}$**), 4.20-4.25 (m, 2H, C$_{hydropy}$-***H*$_{meta}$**). ^{13}C{^{1}H} NMR (101 MHz, C_6D_6): δ 23.26 (P-C(***C***H$_3$)$_2$C$_{hydropy}$), 24.53 (***C*$_{hydropy,para}$**), 31.98 (br, Me of ^{t}Bu), 33.88 (P-C(***C***H$_3$)$_2$C$_{dehydropy}$), 39.14 (C$_{quat}$ of ^{t}Bu), 39.72 (C$_{quat}$ of ^{t}Bu), 47.77 (P-***C***(CH$_3$)$_2$C$_{hydropy}$), 91.35 (vt, J_{PC} = 6.3 Hz, ***C*$_{hydropy,meta}$**), 161.41 (vt, J_{PC} = 6.4 Hz, ***C*$_{hydropy,ortho}$**). ^{31}P{^{1}H} NMR (162 MHz, C_6D_6): δ 71.18. ATR-IR (cm^{-1}): 2964 (m), 2893 (m), 2867 (s), 2732 (s), 2658 (m), 2511 (w), 2467 (w), 2318 (w), 2290 (w), 1191 (w), 1846 (w), 1642 (m), 1595 (w), 1457 (s), 1387 (m), 1365 (m), 1332 (m), 1298 (m), 1245 (w), 1169 (s), 1123 (m), 1024 (m), 933 (m), 895 (m), 809 (m), 718 (m), 687 (m). UV-vis (CH_2Cl_2, [1·10^{-4} M]), λ_{max}, nm (ε, L mol^{-1} cm^{-1}):.242 (28803), 282 (7740), 341 (14606), 466 (1125), 718 (254). ESI-HRMS (*m/z*) calculated for $[C_{27}H_{53}NBrNiP_2]^+$ = 590.2185. Found for $[C_{23}H_{44}NBrNiP_2]^+$ = 590.2172. Despite multiple attempts, satisfactory elemental analysis could not be obtained.

(Me$_4$PNP^{iPr}·H)Ni^{II}H, 9. To a solution of **[1]BPh$_4$** (30 mg, 0.049 mmol) in THF (10 mL) was added a 1M solution of LiBEt$_3$H in THF (98 μL, 0.098 mmol, 2.0 eq.). The solution quickly turns green then dark brown upon addition. The solvent is evaporated, and the solid washed with diethyl ether, the insoluble precipitate is filtered through a short celite pad, and the solvent evaporated to afford a brown solid. We do not report the yield because we could not isolate this complex cleanly, and some side products are still present. ^{1}H NMR (600 MHz, C_6D_6): δ -18.14 (t, J_{PH} = 56.2 Hz, 1H, Ni-***H***), 1.18-1.23 (m, 12H, PCH-C***H*$_3$**), 1.30-1.33 (m 12H, PCH-C***H*$_3$**), 1.41-1.43 (m, 12H, P-C(C***H*$_3$**)$_2$C$_{hydropy}$) 1.93-2.00 (m, 4H, PC***H***-CH$_3$), 3.48-3.50 (td, J_{HH} = 3.4, 1.7 Hz, 2H, C$_{hydropy}$-***H*$_{para}$**), 4.18-4.20 (m, 2H, C$_{hydropy}$-***H*$_{meta}$**). ^{13}C{^{1}H} NMR (151 MHz, C_6D_6): δ 20.28 (PCH-***C***H$_3$), 20.64 (PCH-***C***H$_3$), 24.05 (vt, J_{PC} = 9.8 Hz, P***C***H-CH$_3$), 26.28 (***C*$_{hydropy,para}$**), 26.60 (P-C(***C***H$_3$)$_2$C$_{hydropy}$), P-***C***(CH$_3$)$_2$C$_{hydropy}$), 86.02 (vt, J_{PC} = 5.6 Hz, ***C*$_{hydropy,meta}$**), 161.14 (vt, J_{PC} = 7.7 Hz, ***C*$_{hydropy,ortho}$**). ^{31}P{^{1}H} NMR (162 MHz, C_6D_6): δ 81.10.

[(Me$_4$PNP$^{iPr}_{dearom}$)Ni^{II}Me]$_2$, 10. To a solution of **[5]B(Ar^F)$_4$** (10.4 mg, 0.0078 mmol) in THF at rt, KC_8 (2.3 mg, 0.017 mmol, 2.2 eq.) was added and it was stirred for 1h. The solution was then filtered through a short celite plug and then evaporated to 1 mL and left to crystalize at -30 °C to obtain orange crystals (2.4 mg, 0.0026 mmol, 33%) that were suitable for X-ray diffraction. ^{1}H NMR (400 MHz, C_6D_6): δ -0.56 (t, J_{PH} = 8.2 Hz, 6H, Ni-C***H*$_3$**), 1.11-1.17 (m, 24H, P-C(C***H*$_3$**)$_2$C$_{py}$), 1.44-1.50 (m, 12H, PCH-C***H*$_3$**), 1.50-1.53 (m, 12H, PCH-C***H*$_3$**), 1.51-1.58 (m, 12H, PCH-C***H*$_3$**), 1.56-1.59 (m, 12H, PCH-C***H*$_3$**),

2.03-2.12 (m, 4H, PC***H***-CH_3), 2.16-2.25 (m, 4H, PC***H***-CH_3), 3.26-3.31 (m, 2H, C_{py}-***H*** *para*), 4.49-4.54 (m, 4H, C_{py}-***H*** *meta*). $^{13}C\{^1H\}$ NMR (101 MHz, C_6D_6): δ -22.60 (vt, J_{PC}=24.0 Hz, Ni-***C***H_3), 17.40 (P-C(***C***H_3)$_2$$C_{py}$), 19.42 (P-C(***C***$H_3$)$_2$$C_{py}$), 19.75 (PCH-***C***$H_3$), 20.90 PCH-***C***$H_3$) 22.25 (vt, J_{PC} = 7.5 Hz, P***C***H-CH_3), 24.02 (vt, J_{PC} = 8.5 Hz, P***C***H-CH_3), 24.29 (PCH-***C***H_3), 29.88 (PCH-***C***H_3), 43.20 (***C*** *py,para*), 45.71 (vt, J_{PC} = 8.5 Hz, P-***C***$(CH_3)_2C_{py}$), 90.12 (vt, J_{PC} = 5.8 Hz, ***C*** *py,meta*), 159.27 (vt, J_{PC} = 7.6 Hz, ***C*** *py,ortho*). $^{31}P\{^1H\}$ NMR (162 MHz, C_6D_6): δ 64.43. Despite multiple attempts, satisfactory elemental analysis could not be obtained due to a starting material impurity that could not be completely removed after multiple recrystallizations.

ASSOCIATED CONTENT

SUPPORTING INFORMATION

The Supporting Information is available free of charge on the ACS Publications website.

Experimental details, characterization data, computational details (PDF)

Cartesian coordinates of geometry-optimized structures (XYZ)

Accession Codes

CCDC 1943381−1943394 contain the supplementary crystallographic data for this paper. These data can be obtained free of charge via https://www.ccdc.cam.ac.uk/structures/.

AUTHOR INFORMATION

Corresponding Author

*E-mail: juliak@oist.jp (J.R.K)

ORCID

Sébastien Lapointe : 0000-0003-3190-3803

Eugene Khaskin: 0000-0003-1790-704X

Robert R. Fayzullin : 0000-0002-3740-9833

Julia R. Khusnutdinova: 0000-0002-5911-4382

Notes

The authors declare no competing financial interest.

ACKNOWLEDGMENT

We thank Dr. Michael Roy for support with HRMS, NMR and elemental analysis (OIST). We also thank Dr. Yukio Mizuta (JEOL RESONANCE Inc.) for helpful discussions regarding EPR measurements and simulation. The authors acknowledge the Okinawa Institute of Science and Technology Graduate University for start-up funding and for access to high performing cluster facility.

REFERENCES

(1) Moulton, C. J.; Shaw, B. L., Transition metal–carbon bonds. Part XLII. Complexes of nickel, palladium, platinum, rhodium and iridium with the tridentate ligand 2,6-bis[(di-*t*-butylphosphino)methyl]phenyl. *J. Chem. Soc., Dalton Trans.* **1976**, 1020-1024.

(2) van Koten, G.; Timmer, K.; Noltes, J. G.; Spek, A. L., A novel type of Pt-C interaction and a model for the final stage in reductive elimination processes involving C-C coupling at Pt; synthesis and molecular geometry of [1,N,N'-ε-2,6-bis{(dimethylamino)methyl}-toluene]iodoplatinum(II) tetrafluoroborate. *J. Chem. Soc., Chem. Commun.* **1978**, 250-252.

(3) van Koten, G.; Jastrzebski, J. T. B. H.; Noltes, J. G.; Spek, A. L.; Schoone, J. C., Triorganotin cations stabilized by intramolecular Sn-N coordination; synthesis and characterization of {C,N,N′ -2,6-bis[(dimethylamino)methyl]phenyl}diorganotin bromides. *J. Organomet. Chem.* **1978,** *148*, 233-245.

(4) Castonguay, A.; Sui-Seng, C.; Zargarian, D.; Beauchamp, A. L., Syntheses and Reactivities of New $PCsp_3P$ Pincer Complexes of Nickel. *Organometallics* **2006,** *25*, 602-608.

(5) Kennedy, A. R.; Cross, R. J.; Muir, K. W., Preparation and crystal structure of *trans*-[NiBr{C_6H_3-2,6-$(CH_2PCy_2)_2$}]. *Inorg. Chim. Acta* **1995,** *231*, 195-200.

(6) Huck, W. T. S.; Snellink-Rueel, B.; van Veggel, F. C. J. M.; Reinhoudt, D. N., New Building Blocks for the Noncovalent Assembly of *homo*- and *hetero*-Multinuclear Metallodendrimers. *Organometallics* **1997,** *16*, 4287-4291.

(7) Kozhanov, K. A.; Bubnov, M. P.; Cherkasov, V. K.; Vavilina, N. N.; Efremova, L. Y.; Artyushin, O. I.; Odinets, I. L.; Abakumov, G. A., *o*-Semiquinonic PCP-pincer nickel complexes with alkyl substituents: versatile coordination sphere dynamics. *Dalton Trans.* **2008**, 2849-2853.

(8) Kozhanov, K. A.; Bubnov, M. P.; Cherkasov, V. K.; Fukin, G. K.; Abakumov, G. A., An EPR study of the intramolecular dynamics in *o*-semiquinonic nickel complexes with a diphosphorous pincer ligand. *Chem. Commun.* **2003**, 2610-2611.

(9) Cámpora, J.; Palma, P.; Del Río, D.; Alvarez, E., CO Insertion Reactions into the M-OH Bonds of Monomeric Nickel and Palladium Hydroxides. Reversible Decarbonylation of a Hydroxycarbonyl Palladium Complex. *Organometallics* **2004,** *23*, 1652-1655.

(10) Cámpora, J.; Palma, P.; del Río, D.; Mar Conejo, M.; Alvarez, E., Synthesis and Reactivity of a Mononuclear Parent Amido Nickel Complex. Structures of Ni[C_6H_3-2,6-$(CH_2P$*i*$Pr_2)_2$](NH$_2$) and Ni[C_6H_3-2,6-$(CH_2P$*i*$Pr_2)_2$](OMe). *Organometallics* **2004,** *23*, 5653-5655.

(11) Boro, B. J.; Duesler, E. N.; Goldberg, K. I.; Kemp, R. A., Synthesis, Characterization, and Reactivity of Nickel Hydride Complexes Containing 2,6-$C_6H_3(CH_2PR_2)_2$ (R = tBu, cHex, and iPr) Pincer Ligands. *Inorg. Chem.* **2009,** *48*, 5081-5087.

(12) Groux, L. F.; Belanger-Gariepy, F.; Zargarian, D., Phosphino-indenyl complexes of nickel(II). *Can. J. Chem.* **2005,** *83*, 634-639.

(13) Schmeier, T. J.; Hazari, N.; Incarvito, C. D.; Raskatov, J. A., Exploring the reactions of CO_2 with PCP supported nickel complexes. *Chem. Commun.* **2011,** *47*, 1824-1826.

(14) Levina, V. A.; Rossin, A.; Belkova, N. V.; Chierotti, M. R.; Epstein, L. M.; Filippov, O. A.; Gobetto, R.; Gonsalvi, L.; Lledos, A.; Shubina, E. S.; Zanobini, F.; Peruzzini, M., Acid-Base Interaction between Transition-Metal Hydrides: Dihydrogen Bonding and Dihydrogen Evolution. *Angew. Chem. Int. Ed.* **2011,** *50*, 1367-1370.

(15) van der Boom, M. E.; Liou, S.-Y.; Shimon, L. J. W.; Ben-David, Y.; Milstein, D., Nickel promoted C-H, C-C and C-O bond activation in solution. *Inorg. Chim. Acta* **2004,** *357*, 4015-4023.

(16) Gomez-Benitez, V.; Baldovino-Pantaleon, O.; Herrera-Alvarez, C.; Toscano, R. A.; Morales-Morales, D., High yield thiolation of iodobenzene catalyzed by the phosphinite nickel PCP pincer complex: [NiCl{C_6H_3-2,6-$(OPPh_2)_2$}]. *Tetrahedron Lett.* **2006,** *47*, 5059-5062.

(17) Vabre, B.; Lindeperg, F.; Zargarian, D., Direct, one-pot synthesis of POCOP-type pincer complexes from metallic nickel. *Green Chem.* **2013,** *15*, 3188-3194.

(18) Lapointe, S.; Vabre, B.; Zargarian, D., POCOP-Type Pincer Complexes of Nickel: Synthesis, Characterization, and

Ligand Exchange Reactivities of New Cationic Acetonitrile Adducts. *Organometallics* **2015,** *34*, 3520-3531.

(19) Estudiante-Negrete, F.; Hernandez-Ortega, S.; Morales-Morales, D., Ni(II)-POCOP pincer compound [NiCl{$C_{10}H_5$-2,10-($OPPh_2$)$_2$}] an efficient and robust nickel catalyst for the Suzuki-Miyaura coupling reactions. *Inorg. Chim. Acta* **2012,** *387*, 58-63.

(20) Chakraborty, S.; Krause, J. A.; Guan, H., Hydrosilylation of Aldehydes and Ketones Catalyzed by Nickel PCP-Pincer Hydride Complexes. *Organometallics* **2009,** *28*, 582-586.

(21) Zhang, J.; Medley, C. M.; Krause, J. A.; Guan, H., Mechanistic Insights into C-S Cross-Coupling Reactions Catalyzed by Nickel Bis(phosphinite) Pincer Complexes. *Organometallics* **2010,** *29*, 6393-6401.

(22) Chakraborty, S.; Patel, Y. J.; Krause, J. A.; Guan, H., Catalytic properties of nickel bis(phosphinite) pincer complexes in the reduction of CO_2 to methanol derivatives. *Polyhedron* **2012,** *32*, 30-34.

(23) Pandarus, V.; Zargarian, D., New Pincer-Type Diphosphinito (POCOP) Complexes of Nickel. *Organometallics* **2007,** *26*, 4321-4334.

(24) Spasyuk, D. M.; Zargarian, D.; van der Est, A., New POCN-Type Pincer Complexes of Nickel(II) and Nickel(III). *Organometallics* **2009,** *28*, 6531-6540.

(25) Zhang, B.-S.; Wang, W.; Shao, D.-D.; Hao, X.-Q.; Gong, J.-F.; Song, M.-P., Unsymmetrical Chiral PCN Pincer Palladium(II) and Nickel(II) Complexes of (Imidazolinyl)aryl Phosphinite Ligands: Synthesis via Ligand C-H Activation, Crystal Structures, and Catalytic Studies. *Organometallics* **2010,** *29*, 2579-2587.

(26) Spasyuk, D. M.; Gorelsky, S. I.; van der Est, A.; Zargarian, D., Characterization of Divalent and Trivalent Species Generated in the Chemical and Electrochemical Oxidation of a Dimeric Pincer Complex of Nickel. *Inorg. Chem.* **2011,** *50*, 2661-2674.

(27) Yang, M.-J.; Liu, Y.-J.; Gong, J.-F.; Song, M.-P., Unsymmetrical Chiral PCN Pincer Palladium(II) and Nickel(II) Complexes with Aryl-Based Aminophosphine-Imidazoline Ligands: Synthesis via Aryl C-H Activation and Asymmetric Addition of Diarylphosphines to Enones. *Organometallics* **2011,** *30*, 3793-3803.

(28) Sanford, J.; Dent, C.; Masuda, J. D.; Xia, A., Synthesis, characterization and application of pincer-type nickel iminophosphinite complexes. *Polyhedron* **2011,** *30*, 1091-1094.

(29) Fan, L.; Foxman, B. M.; Ozerov, O. V., N-H Cleavage as a Route to Palladium Complexes of a New PNP Pincer Ligand. *Organometallics* **2004,** *23*, 326-328.

(30) Ozerov, O. V.; Guo, C.; Fan, L.; Foxman, B. M., Oxidative Addition of N-C and N-H Bonds to Zerovalent Nickel, Palladium, and Platinum. *Organometallics* **2004,** *23*, 5573-5580.

(31) Liang, L.-C.; Chien, P.-S.; Huang, Y.-L., Intermolecular Arene C-H Activation by Nickel(II). *J. Am. Chem. Soc.* **2006,** *128*, 15562-15563.

(32) Liang, L.-C.; Chien, P.-S.; Lin, J.-M.; Huang, M.-H.; Huang, Y.-L.; Liao, J.-H., Amido Pincer Complexes of Nickel(II): Synthesis, Structure, and Reactivity. *Organometallics* **2006,** *25*, 1399-1411.

(33) Adhikari, D.; Huffman, J. C.; Mindiola, D. J., Structural elucidation of a nickel boryl complex. A recyclable borylation Ni(II) reagent of bromobenzene. *Chem. Commun.* **2007**, 4489-4491.

(34) Adhikari, D.; Pink, M.; Mindiola, D. J., Mild protocol for the synthesis of stable nickel complexes having primary and secondary silyl ligands. *Organometallics* **2009,** *28*, 2072-2077.

(35) Fryzuk, M. D.; Montgomery, C. D., Amides of the platinum group metals. *Coord. Chem. Rev.* **1989,** *95*, 1-40.

(36) Ingleson, M. J.; Fullmer, B. C.; Buschhorn, D. T.; Fan, H.; Pink, M.; Huffman, J. C.; Caulton, K. G., Influence of the d-Electron Count on CO Binding by Three-Coordinate [($tBu_2PCH_2SiMe_2$)$_2$N]Fe, -Co, and -Ni. *Inorg. Chem.* **2008,** *47*, 407-409.

(37) Fryzuk, M. D.; MacNeil, P. A., Hybrid multidentate ligands. Tridentate amidophosphine complexes of nickel(II) and palladium(II). *J. Am. Chem. Soc.* **1981,** *103*, 3592-3.

(38) Tondreau, A. M.; Boncella, J. M., The synthesis of PNP-supported low-spin nitro manganese(I) carbonyl complexes. *Polyhedron* **2016,** *116*, 96-104.

(39) Abdul Goni, M.; Rosenberg, E.; Meregude, S.; Abbott, G., A methods study of immobilization of PONOP pincer transition metal complexes on silica polyamine composites (SPC). *J. Organomet. Chem.* **2016,** *807*, 1-10.

(40) Castro-Rodrigo, R.; Chakraborty, S.; Munjanja, L.; Brennessel, W. W.; Jones, W. D., Synthesis, Characterization, and Reactivities of Molybdenum and Tungsten PONOP Pincer Complexes. *Organometallics* **2016,** *35*, 3124-3131.

(41) DeRieux, W.-S. W.; Wong, A.; Schrodi, Y., Synthesis and characterization of iron complexes based on bis-phosphinite PONOP and bis-phosphite PONOP pincer ligands. *J. Organomet. Chem.* **2014,** *772-773*, 60-67.

(42) Kundu, S.; Brennessel, W. W.; Jones, W. D., Synthesis and Reactivity of New Ni, Pd, and Pt 2,6-Bis(di-*tert*-butylphosphinito)pyridine Pincer Complexes. *Inorg. Chem.* **2011,** *50*, 9443-9453.

(43) Kundu, S.; Brennessel, W. W.; Jones, W. D., Making M-CN bonds from M-Cl in (PONOP)M and (dippe)Ni systems (M = Ni, Pd, and Pt) using *t*-BuNC. *Inorg. Chim. Acta* **2011,** *379*, 109-114.

(44) Salem, H.; Shimon, L. J. W.; Diskin-Posner, Y.; Leitus, G.; Ben-David, Y.; Milstein, D., Formation of Stable trans-Dihydride Ruthenium(II) and 16-Electron Ruthenium(0) Complexes Based on Phosphinite PONOP Pincer Ligands. Reactivity toward Water and Electrophiles. *Organometallics* **2009,** *28*, 4791-4806.

(45) Barloy, L.; Malaise, G.; Ramdeehul, S.; Newton, C.; Osborn, J. A.; Kyritsakas, N., Synthesis and Structural Studies of Binuclear Platinum(II) Complexes with a Novel Phosphorus-Nitrogen-Phosphorus Ligand. *Inorg. Chem.* **2003,** *42*, 2902-2907.

(46) Vabre, B.; Canac, Y.; Duhayon, C.; Chauvin, R.; Zargarian, D., Nickel(II) complexes of the new pincer-type unsymmetrical ligands PIMCOP, PIMIOCOP, and NHCCOP: versatile binding motifs. *Chem. Commun.* **2012,** *48*, 10446-10448.

(47) Vechorkin, O.; Proust, V.; Hu, X., Functional Group Tolerant Kumada-Corriu-Tamao Coupling of Nonactivated Alkyl Halides with Aryl and Heteroaryl Nucleophiles: Catalysis by a Nickel Pincer Complex Permits the Coupling of Functionalized Grignard Reagents. *J. Am. Chem. Soc.* **2009,** *131*, 9756-9766.

(48) Madhira, V. N.; Ren, P.; Vechorkin, O.; Hu, X.; Vicic, D. A., Synthesis and electronic properties of a pentafluoroethyl-derivatized nickel pincer complex. *Dalton Trans.* **2012,** *41*, 7915-7919.

(49) Breitenfeld, J.; Scopelliti, R.; Hu, X., Synthesis, Reactivity, and Catalytic Application of a Nickel Pincer Hydride Complex. *Organometallics* **2012,** *31*, 2128-2136.

(50) van Koten, G.; Milstein, D., *Organometallic pincer chemistry*. 1st ed.; Springer: Berlin; New York, 2013; p 356.

(51) Alig, L.; Fritz, M.; Schneider, S., First-Row Transition Metal (De)Hydrogenation Catalysis Based On Functional Pincer Ligands. *Chem. Rev.* **2019,** *119*, 2681-2751.

(52) Morales-Morales, D.; Jensen, C. M., *The chemistry of pincer compounds*. Elsevier: Amsterdam; Boston, 2007.

(53) Mukherjee, A.; Milstein, D., Homogeneous Catalysis by Cobalt and Manganese Pincer Complexes. *ACS Catal.* **2018,** *8*, 11435-11469.

(54) Valdés, H.; García-Eleno, M. A.; Canseco-Gonzalez, D.; Morales-Morales, D., Recent Advances in Catalysis with Transition-Metal Pincer Compounds. *ChemCatChem* **2018,** *10*, 3136-3172.

(55) Kumar, A.; Bhatti, T. M.; Goldman, A. S., Dehydrogenation of Alkanes and Aliphatic Groups by Pincer-Ligated Metal Complexes. *Chem. Rev.* **2017,** *117*, 12357-12384.

(56) Lawrence, M. A. W.; Green, K.-A.; Nelson, P. N.; Lorraine, S. C., Review: Pincer ligands—Tunable, versatile and applicable. *Polyhedron* **2018,** *143*, 11-27.

(57) Rettenmeier, C. A.; Wadepohl, H.; Gade, L. H., Electronic structure and reactivity of nickel(I) pincer complexes: their aerobic transformation to peroxo species and site selective C-H oxygenation. *Chem. Sci.* **2016,** *7*, 3533-3542.

(58) Rettenmeier, C. A.; Wadepohl, H.; Gade, L. H., Structural Characterization of a Hydroperoxo Nickel Complex and Its Autoxidation: Mechanism of Interconversion between Peroxo, Superoxo, and Hydroperoxo Species. *Angew. Chem. Int. Ed.* **2015,** *54*, 4880-4884.

(59) Chakraborty, S.; Zhang, J.; Krause, J. A.; Guan, H., An Efficient Nickel Catalyst for the Reduction of Carbon Dioxide with a Borane. *J. Am. Chem. Soc.* **2010,** *132*, 8872-8873.

(60) Li, H.; Gonçalves, T. P.; Hu, J.; Zhao, Q.; Gong, D.; Lai, Z.; Wang, Z.; Zheng, J.; Huang, K.-W., A Pseudodearomatized $PN_3P^*Ni–H$ Complex as a Ligand and σ-Nucleophilic Catalyst. *J. Org. Chem.* **2018,** *83*, 14969-14977.

(61) Wenz, J.; Wadepohl, H.; Gade, L. H., Regioselective hydrosilylation of epoxides catalysed by nickel(II) hydrido complexes. *Chem. Commun.* **2017,** *53*, 4308-4311.

(62) Eberhardt, N. A.; Wellala, N. P. N.; Li, Y.; Krause, J. A.; Guan, H., Dehydrogenative Coupling of Aldehydes with Alcohols Catalyzed by a Nickel Hydride Complex. *Organometallics* **2019,** *38*, 1468-1478.

(63) Chakraborty, S.; Zhang, J.; Patel, Y. J.; Krause, J. A.; Guan, H., Pincer-ligated nickel hydridoborate complexes: the dormant species in catalytic reduction of carbon dioxide with boranes. *Inorg. Chem.* **2013,** *52*, 37-47.

(64) Wilson, G. L. O.; Abraha, M.; Krause, J. A.; Guan, H., Reactions of phenylacetylene with nickel POCOP-pincer hydride complexes resulting in different outcomes from their palladium analogues. *Dalton Trans.* **2015,** *44*, 12128-12136.

(65) Jonasson, K. J.; Wendt, O. F., Synthesis and Characterization of a Family of POCOP Pincer Complexes with Nickel: Reactivity Towards CO_2 and Phenylacetylene. *Chem. Eur. J.* **2014,** *20*, 11894-11902.

(66) Wellala, N. P. N.; Dong, H. T.; Krause, J. A.; Guan, H., Janus POCOP Pincer Complexes of Nickel. *Organometallics* **2018,** *37*, 4031-4039.

(67) Mousa, A. H.; Bendix, J.; Wendt, O. F., Synthesis, characterization, and reactivity of PCN pincer nickel complexes. *Organometallics* **2018,** *37*, 2581-2593.

(68) Csok, Z.; Vechorkin, O.; Harkins, S. B.; Scopelliti, R.; Hu, X., Nickel complexes of a pincer NN_2 ligand: multiple carbon-chloride activation of CH_2Cl_2 and $CHCl_3$ leads to selective carbon-carbon bond formation. *J. Am. Chem. Soc.* **2008,** *130*, 8156-8157.

(69) Khusnutdinova, J. R.; Milstein, D., Metal-Ligand Cooperation. *Angew. Chem. Int. Ed.* **2015,** *54*, 12236-12273.

(70) Vogt, M.; Rivada-Wheelaghan, O.; Iron, M. A.; Leitus, G.; Diskin-Posner, Y.; Shimon, L. J. W.; Ben-David, Y.; Milstein, D., Anionic Nickel(II) Complexes with Doubly Deprotonated PNP Pincer-Type Ligands and Their Reactivity toward CO_2. *Organometallics* **2013,** *32*, 300-308.

(71) Yoo, C.; Kim, Y.-E.; Lee, Y., Selective Transformation of CO_2 to CO at a Single Nickel Center. *Acc. Chem. Res.* **2018,** *51*, 1144-1152.

(72) Sahoo, D.; Yoo, C.; Lee, Y., Direct CO2 Addition to a Ni(0)–CO Species Allows the Selective Generation of a Nickel(II) Carboxylate with Expulsion of CO. *J. Am. Chem. Soc.* **2018,** *140*, 2179-2185.

(73) Anderson, T. J.; Jones, G. D.; Vicic, D. A., Evidence for a Ni(I) Active Species in the Catalytic Cross-Coupling of Alkyl Electrophiles. *J. Am. Chem. Soc.* **2004,** *126*, 8100-8101.

(74) Zimmermann, P.; Limberg, C., Activation of Small Molecules at Nickel(I) Moieties. *J. Am. Chem. Soc.* **2017,** *139*, 4233-4242.

(75) Scheller, S.; Goenrich, M.; Boecher, R.; Thauer, R. K.; Jaun, B., The key nickel enzyme of methanogenesis catalyses the anaerobic oxidation of methane. *Nature* **2010,** *465*, 606-608.

(76) Ragsdale, S. W., Nickel-based Enzyme Systems. *J. Biol. Chem.* **2009,** *284*, 18571-18575.

(77) Lapointe, S.; Khaskin, E.; Fayzullin, R. R.; Khusnutdinova, J. R., Stable Nickel(I) Complexes with Electron-Rich, Sterically-Hindered, Innocent PNP Pincer Ligands. *Organometallics* **2019,** *38*, 1581-1594.

(78) Rosiak, D.; Okuniewski, A.; Chojnacki, J., Novel complexes possessing Hg–(Cl, Br, I)···OC halogen bonding and unusual $Hg_2S_2(Br/I)_4$ kernel. The usefulness of τ_4' structural parameter. *Polyhedron* **2018,** *146*, 35-41.

(79) Yang, L.; Powell, D. R.; Houser, R. P., Structural variation in copper(I) complexes with pyridylmethylamide ligands: structural analysis with a new four-coordinate geometry index, τ_4. *Dalton Trans.* **2007**, 955-964.

(80) Gwak, J.; Ahn, S.; Baik, M.-H.; Lee, Y., One metal is enough: a nickel complex reduces nitrate anions to nitrogen gas. *Chem. Sci.* **2019,** *10*, 4767-4774.

(81) Ohtsu, H.; Tanaka, K., An Organic Hydride Transfer Reaction of a Ruthenium NAD Model Complex Leading to Carbon Dioxide Reduction. *Angew. Chem. Int. Ed.* **2012,** *51*, 9792-9795.

(82) Fukushima, T.; Ghosh, D.; Kobayashi, K.; Ohtsu, H.; Kitagawa, S.; Tanaka, K., Four-Electron Reduction of a New Ruthenium Dicarbonyl Complex Having Two NAD Model Ligands through Decarboxylation in Water. *Inorg. Chem.* **2016,** *55*, 11613-11616.

(83) Ohtsu, H.; Fujii, S.; Tsuge, K.; Tanaka, K., Novel synthesis of a four-electron-reduced ruthenium(II) NADH-type complex under water-gas-shift reaction conditions. *Dalton Trans.* **2016,** *45*, 16130-16133.

(84) Connelly, N. G.; Geiger, W. E., Chemical Redox Agents for Organometallic Chemistry. *Chem. Rev.* **1996,** *96*, 877-910.

(85) Zanello, P., *Inorganic electrochemistry : theory, practice and applications*. Royal Society of Chemistry: Cambridge, 2003.

(86) Jones, G. D.; Martin, J. L.; McFarland, C.; Allen, O. R.; Hall, R. E.; Haley, A. D.; Brandon, R. J.; Kanovalova, T.; Desrochers, P. J.; Pulay, P.; Vicic, D. A., Ligand Redox Effects in the Synthesis, Electronic Structure, and Reactivity of an Alkyl-Alkyl Cross-Coupling Catalyst. *J. Am. Chem. Soc.* **2006,** *128*, 13175-13183.

(87) Yarkov SP, B. V., Zubarev VE, Spin trap in study of acetone radiolysis using nitrones. *Khim. Vys. Energ.* **1980,** *14*, 115-120.

(88) Yoo, C.; Lee, Y., A T-Shaped Nickel(I) Metalloradical Species. *Angew. Chem. Int. Ed.* **2017,** *56*, 9502-9506.

(89) Hamilton, D. E.; Drago, R. S.; Telser, J., Spin trapping of a cobalt-dioxygen complex. *J. Am. Chem. Soc.* **1984,** *106*, 5353-5355.

(90) Khusnutdinova, J. R.; Rath, N. P.; Mirica, L. M., The Aerobic Oxidation of a Pd(II) Dimethyl Complex Leads to Selective Ethane Elimination from a Pd(III) Intermediate. *J. Am. Chem. Soc.* **2012,** *134*, 2414-2422.

(91) Sheldrick, G., SHELXT - Integrated space-group and crystal-structure determination. *Acta Crystallogr., Sect. A: Found. Adv.* **2015,** *71*, 3-8.

(92) Sheldrick, G., Crystal structure refinement with SHELXL. *Acta Crystallogr., Sect. C: Struct. Chem.* **2015,** *71*, 3-8.

(93) Spek, A., PLATON SQUEEZE: a tool for the calculation of the disordered solvent contribution to the calculated structure factors. *Acta Crystallogr., Sect. C: Struct. Chem.* **2015,** *71*, 9-18.